Journal of Theoretical Biology 510 (2021) 110525

Contents lists available at ScienceDirect

Journal of Theoretical Biology

journal homepage: www.elsevier.com/locate/yjtbi

Lepidopteran mouthpart architecture suggests a new mechanism of fluid uptake by insects with long proboscises

Artur A. Salamatin [a,1], Peter H. Adler [b], Konstantin G. Kornev [c,*]

[a] 18 Kremlyovskaya str, Institute of Geology and Petroleum Technologies & Institute of Computational Mathematics and Information Technologies, Kazan Federal University, Kazan, Tatarstan 420008, Russia
[b] 130 McGinty Court, E-143 Poole Agricultural Center, Dept. of Plant and Environmental Sciences, Clemson University, Clemson, SC 29634, USA
[c] 515 Calhoun Drive, 161 Sirrine Hall, Dept. of Materials Science and Engineering, Clemson University, Clemson South Carolina 29634, USA

ARTICLE INFO

Article history:
Received 24 April 2020
Revised 7 September 2020
Accepted 6 October 2020
Available online 14 October 2020

Keywords:
Fluid-feeding
Insect proboscis
Capillarity
Flow modeling
Evolution

ABSTRACT

Proboscises of many fluid-feeding insects share a common architecture: they have a partially open food canal along their length. This feature has never been discussed in relation to the feeding mechanism. We formulated and solved a fluid mechanics model of fluid uptake and estimated the time required to completely fill the food canal of the entire proboscis through the openings along its length. Butterflies and moths are taken as illustrative and representative of fluid-feeding insects. We demonstrated that the proposed mechanism of filling the proboscis with fluid through permeable lengthwise bands, in association with a thin film of saliva in the food canal, offers a competitive pathway for fluid uptake. Compared with the conventional mechanism of fluid uptake through apically restricted openings, the new mechanism provides a faster rate of fluid uptake, especially for long-tongued insects. Accordingly, long-tongued insects with permeable lengthwise bands would be able to more rapidly exploit a broader range of liquids in the form of films, pools, and discontinuous columns, thereby conserving energy and minimizing exposure to predators, particularly for hovering insects.

1. Introduction

Insects that acquire fluids through a proboscis are remarkably successful, if success is evaluated in terms of sheer numbers. Nearly half of all known insects—roughly half a million species—take up fluid through a proboscis (Shaw, 2014; Adler and Foottit, 2017; Grimaldi and Engel, 2005). An understanding of the evolutionary diversification of insects and their feeding organs requires knowledge of device structure, function, and performance (Lauder et al., 2003; Russell, 1916; Krenn and Aspock, 2012; Wainwright, 2007; Munoz, 2019). Many insects can acquire a highly viscous liquid such as honey or an almost inviscid mineral water at astonishingly high rates (Kingsolver and Daniel, 1995; Krenn, 2010; Smith, 1979; Smith and Gilbert, 1985; Borrell and Krenn, 2006; Adler, 1982; Wigglesworth, 1972; Eisner, 2005). Fluid feeding with a proboscis has been divided into four steps: i) proboscis wetting and ii) dewetting, iii) fluid absorbing, and iv) fluid pumping through the food canal by a sucking pump (Kornev and Adler, 2019) (Fig. 1). Behavioral strategies used to load (i.e., wet and dewet) the proboscis with liquid are not necessarily connected with the four steps of the fluid-feeding model, which specify actual physico-chemical determinants of fluid flow from the liquid source to the food canal and finally to the sucking pump. The insect's behavioral strategy depends primarily on the external organization of its proboscis. For example, butterflies and moths drink through tubular proboscises (Krenn, 2010), flies mop up fluid with sponge-like proboscises (Kingsolver and Daniel, 1995; Smith and Gilbert, 1985), and bees lap up fluid with hairy proboscises; these insects must then deliver the fluid load to the food canal (Shi et al., 2020).

The four-step model can flexibly accommodate the various structural features of the proboscises of different insect groups. Unlike the tubular proboscises of butterflies and moths in which fluid directly enters the food canal (absorption) after loading (wetting and dewetting), the proboscises of flies and bees involve two phases in the absorption step. In the initial phase, the spongy end of the fly proboscis takes fluid into the pseudotracheal channels, and the hairy proboscis of the bee holds the fluid between the hairs. Thus, for flies and bees, the wetting and dewetting steps, together with the initial phase of absorption by the pseudotracheae and hairs, load the fluid before the final phase of absorption when the fluid actually enters and fills the food canal in the first

* Corresponding author.
E-mail addresses: asalama@clemson.edu (A.A. Salamatin), padler@clemson.edu (P.H. Adler), kkornev@clemson.edu (K.G. Kornev).
[1] ORCID: 0000-0002-1099-4016.

https://doi.org/10.1016/j.jtbi.2020.110525
0022-5193/

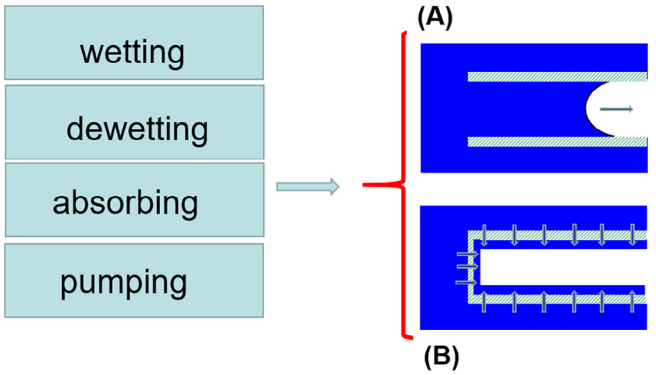

Fig. 1. Four steps of fluid uptake by insects with proboscises: wetting, dewetting, absorbing, and pumping. The absorption step ends when the food canal becomes filled with a liquid column or a bubble train (Kornev and Adler, 2019; Monaenkova et al., 2012), formed from the first sip by an insect. (A) The drinking-straw model assumes that the proboscis as a cylindrical tube (shown schematically in longitudinal section as two hatched slabs) is dipped in a liquid reservoir (blue), and the food-canal filling occurs by spontaneous movement of a liquid meniscus that is nucleated at the proboscis tip. This meniscus would drag the liquid column toward the sucking pump in the direction shown by the arrow. (B) In our proposed model, the filling of the food canal occurs through permeable slits (vertical arrows) running along the length of the proboscis. Fluid also can enter minute slits even at the putatively sealed tip of the proboscis (horizontal arrows). In contrast to the drinking-straw model (A), fluid does not need to travel from the tip to the sucking pump; the food canal will be filled as soon as the air bubble (white) disappears. In both cases, flow is caused by capillary action, and the sucking pump does not need to be involved, thereby conserving energy. To bring fluid to the sucking pump, the insect needs to spend energy. (For interpretation of the references to color in this figure legend, the reader is referred to the web version of this article.)

sip. Despite significant progress in understanding the fluid-loading mechanisms of bees and flies (Shi et al., 2020; Krenn, 2019; Nasto et al., 2018; Lechantre et al., 2019), it remains unclear how the loaded fluid enters the food canal and how much time is required to fill the food canal in this final phase of the absorption step (Smith and Gilbert, 1985).

Fluid entering and filling the food canal is a critical component of the absorption step, and in many cases, it is the time-limiting step for food acquisition by insects that visit different food patches while needing to conserve energy (Charnov, 1976; Johnson et al., 2017). Hovering insects, such as hawk moths and certain flies, with long proboscises are also subject to predation and, hence, might not be able to afford staying at the same food patch for long (Wasserthal, 1997; Pauw et al., 2009; Arditti et al., 2012; Josens and Farina, 2001; Danaher et al., 2019). Here, our primary attention is given to the analysis of the mechanism of fluid entry into the food canal of the lepidopteran proboscis, with possible application to other long-tongued insects with similar structural arrangement of the proboscis. We do not address groups of fluid-feeding insects such as flies with pseudotracheae or most bees and other hymneopterans.

The step requiring food-canal filling was conventionally analyzed using a drinking-straw model (Kingsolver and Daniel, 1995; Daniel and Kingsolver, 1983; Daniel et al., 1989; Kim et al., 2011), which assumes that liquid enters the food canal through the tip and moves towards the head under the pressure differential created by the meniscus and external source of the liquid (Kingsolver and Daniel, 1995) (Fig. 1a). Some Lepidoptera are able to open up the tip of their proboscises by sliding their galeae in antiparallel movements (Tsai et al., 2014). Therefore, this mechanism should be considered when evaluating the time required to fill the food canal.

When the food canal has been filled, the liquid column moves up the food canal into the gut by the action of the sucking pump in the head, representing the fourth step in our four-step model. The performance of insect fluid feeders has been evaluated on the basis of the Hagen-Poiseuille theory of fluid flow through a circular tube (Krenn, 2010; Borrell and Krenn, 2006; Daniel and Kingsolver, 1983; Daniel et al., 1989; Kim et al., 2011; Kingsolver and Daniel, 1979). This evaluation allows the sucking pump in the head of the insect to be decoupled from the proboscis. However, estimates of the driving pressure in the pump (Smith and Gilbert, 1985; Bennet-Clark, 1963; Lehane, 2005; Tsai et al., 2014), X-ray phase-contrast imaging experiments (Westneat et al., 2008; Monaenkova et al., 2012; Lee et al., 2014; Kornev et al., 2016), and neurophysiological analysis of the pump (Davis and Hildebrand, 2006) have revealed the complexity of its structure and the liquid flow, drawing into question the applicability of the Hagen-Poiseuille law for evaluation of the pumping scenario.

We develop a model of fluid uptake through the slits along insect proboscises. As a model group of insects, we consider Lepidoptera (butterflies and moths). The model choice is based on recent observations of fluid uptake by Lepidoptera, using optical microscopy and X-ray phase-contrast imaging (Tsai et al., 2014; Monaenkova et al., 2012; Lee et al., 2014a, 2014b; Kwauk et al., 2014; Lee and Lee, 2014; Zhang et al., 2018) and a rich set of morphological data available for these insects (Krenn, 2019).

We show that two principal factors control fluid intake: permeability of the lengthwise bands of slits and viscous resistance of the films spreading along the food canal. First, we discuss the scenario when fluid uptake is limited by permeability of the slits in the lengthwise bands. We then examine the scenario when fluid uptake is limited by viscous resistance of the film spreading over the walls of the food canal. The structural determinants of proboscises of various lepidopteran species are discussed and a classification of flow regimes with respect to the proposed structural determinants is proposed. We suggest that the fluid-flow scenarios developed for butterflies and moths can be applied to additional groups of long-tongued fluid-feeding insects.

2. An example of the proboscis with lengthwise permeable bands: Butterflies and moths

We focus on the lepidopteran proboscis, given that it is the most-studied among long-tongued insects with lengthwise permeable bands of slits. The lepidopteran proboscis is a long tube formed by paired strands, the galeae, held together by an array of hook-like legulae at the ventral side of the proboscis and another array of shingle-like legulae at the dorsal side (Krenn, 2010; Lehnert et al., 2016, 2013; Krenn and Bauder, 2018) (Fig. 2). We refer to these two pairs of parallel arrays of legulae as the “legular bands”. Each galea has C-type concave walls, which form the food canal when the galeae are united.

X-ray phase-contrast and optical microscopy of drop penetration into the food canal has revealed that fluid enters through the legular bands (Monaenkova et al., 2012). These observations were supported by an analysis of spontaneous withdrawal of liquid from fluid pools and films (Tsai et al., 2014; Monaenkova et al., 2012; Lee et al., 2014a, 2014b; Kwauk et al., 2014; Lee and Lee, 2014; Zhang et al., 2018). The findings imply, first, that the legular bands are porous and permeable to liquid and, second, that a suction pressure drop is built up spontaneously as the liquid contacts the legular bands. Proboscis morphology (Tsai et al., 2011; Krenn and Muhlberger, 2002; Krenn et al., 2001; Mollemann et al., 2005) and the specifics of legular bands have been reviewed for many lepidopterans to confirm that the porosity of the proboscis is a common feature among species. The data on morphological features of selected lepidopteran proboscises related to fluid uptake are summarized in Table 1. The permeability of legular bands of the proboscis was determined experimentally only for the Monarch butterfly (Monaenkova et al., 2012).

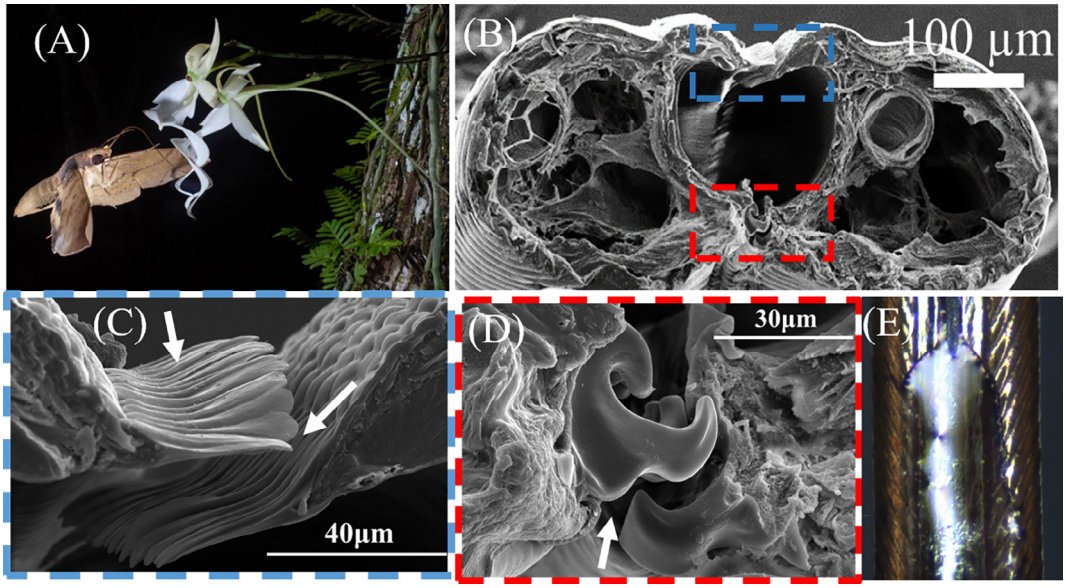

Fig. 2. A) Hawk moth (*Pachylia ficus*) nectaring on *Dendrophylax lindenii* (Danaher et al., 2019). B) SEM micrograph of the cross-section of the proboscis of *Manduca sexta*, with the dorsal (C) and ventral (D) legular bands. The liquid can flow between individual legulae or between the fence-like rows of legulae. Arrows show these flow directions. (D) The liquid can penetrate the ventral legular band through the space between the legulae, indicated by the arrow. (E) A drop of methylene blue-dyed water sinks through the dorsal legular bands. B–E adapted from (Zhang et al., 2018). (For interpretation of the references to color in this figure legend, the reader is referred to the web version of this article.)

The proboscis of most Lepidoptera is divided structurally and functionally into a distal drinking region of about 5–20% of the proboscis length, where the legulae are widely spaced, and a large proximal non-drinking region, where the legulae and the legular bands are more tightly appressed (Pometto et al., 2020). We emphasize that the values for permeability $k \sim 10^{-15}$ m^2 in Table 1 are taken for the non-drinking region about 10 mm from the junction of the Monarch butterfly proboscis with the head (Monaenkova et al., 2012), not from the more widely spaced legulae in the drinking region. Owing to the lack of data for other Lepidoptera, we fix this value of permeability and use it as a conservative estimate, relative to the greater permeability in the drinking region, for the other lepidopteran species in Table 1.

The width of the two legular bands, $2w$, varies among species, but its ratio to the perimeter of the food canal cross-section of a single galea, $w/\pi R$, is always <1 (Table 1). The majority of species have the ratio $w/\pi R$ within the range of 0.1–0.2; only two species in this table, *Ethmia dodecea* (Elachistidae) and *Synathedon vespiformis* (Sesiidae), have a ratio above 0.3. The typical thickness of the proboscis wall near the legular bands is small, spanning an interval from $l \sim 3$ µm to 10 µm. Only the hawk moth *Manduca sexta* has a markedly thick wall, $l \sim 20$ µm.

When the insect applies its proboscis to a liquid in a pool or a film or by piercing tissue, the external surface of the proboscis becomes covered with a liquid film. To approximately estimate the rate of fluid uptake and penetration through the permeable bands, we ignore the inhomogeneity of film thickness along the proboscis axis. The food canal is considered as an infinitely long circular cylinder of radius R. Thus, a two-dimensional (2D) flow at each arbitrarily chosen cross-section perpendicular to the proboscis looks the same as schematically shown in Fig. 3.

We introduce a polar system of coordinates (r, θ), with the origin at the center of the food canal, and make the counterclockwise direction positive for measurements of angle θ (Fig. 3 A). The legular bands are placed at $\theta = \pm \pi/2$. We assume that the dorsal and ventral legular bands have the same permeability.

The legular bands and the surface of the food canal are hydrophilic, and to maintain proboscis functionality, butterflies and moths, wet the legular bands and the food canal with saliva (Zhang et al., 2018a, 2018b; Krenn, 1997; Pometto et al., 2020). Thus, an infinitesimally thin layer of saliva is present on the surface of the food canal. Therefore, immediately after contacting the legular band, the liquid food is subject to the capillary pressure of the infinitesimally thin film of saliva covering the food canal from inside.

To estimate the driving capillary pressure, we use the Laplace law of capillarity (Vogel, 2003) relating the pressure p in the internal film to the air pressure in the food canal. If we assume that the air pressure is the same as that in the pool of liquid, p_{atm} , for a film of uniform thickness h, the Laplace law is written as

$$p - p_{atm} = -\frac{\sigma}{R-h}, \tag{1}$$

where σ is the surface tension of the air/liquid interface. The negative sign in Eq. (1) indicates that the pressure in the internal film is below atmospheric pressure. This suction pressure drives the liquid from the pool into the food canal; the thicker the film, the greater the suction pressure.

3. Flow scenarios

Fluid conductivity of the legular bands. The overall flux through the legular bands is determined by the permeability k entering Darcy's law (Vogel, 2003, 1996) which relates the flow velocity q with the pressure differential (1) as follows

$$q = -\frac{k}{\eta}\frac{p - p_{atm}}{l} \tag{2}$$

where, l is the thickness of the legular band of the proboscis, and η is the liquid viscosity. The permeability k is a characteristic materials parameter of a given insect; it is assumed to be independent of the applied pressure differential.

Substituting Eq. (1) into Darcy's law (2), and multiplying both sides by the width w of the legular band, we obtain the following estimate for the volumetric flow rate per unit length of the proboscis:

Table 1
Morphological characteristics of proboscises of various Lepidoptera species. Dimensionless permeability Q was estimated assuming that the legular bands have slit-like pores with the pore opening of 100 nm, resulting in $k \sim 10^{-15}$ m^2.

Species (Family)[d]	Radius of the food canal, R, μm	Wall thickness in the permeable part of legular bands, l, μm	Width of the permeable part of legular bands, w, μm	Reference filling time [a,b,] T_{ref}, ms	Pressure differential [b,] σ/R, atm	Dimensionless width of the permeable part of the legular bands, $w/\pi R$	Dimensionless permeability of the legular bands [a,] $Q \times 10^6$
Manduca sexta (Sphingidae) (Zhang et al., 2018)	80.7	18.2	23.8	9000[c]	0.0087	0.1	0.2
Idea leuconoe (Nymphalidae) (Tsai et al., 2011)	40	11.5	17.2	970	0.017	0.14	0.93
Heliconius melpomene (Nymphalidae) (Tsai et al., 2014)	40	10.5	18.1	840	0.017	0.14	1.1
Pieris brassicae (Pieridae) (Tsai et al., 2014)	39	5.63	11.2	670	0.02	0.1	1.3
Damas clavus (Hesperiidae) (Krenn and Bauder, 2018)	30.3	8.4	10.8	490	0.023	0.11	1.4
Archaeoprepona demophon (Nymphalidae) (Tsai et al., 2014)	32	6.3	12	400	0.02	0.12	1.8
Vanessa cardui (Nymphalidae) (Krenn, 2010; Tsai et al., 2014)	39.7	10.4	31.9	460	0.018	0.26	2
Siproeta stelenes (Nymphalidae) (Tsai et al., 2014)	32	8.4	19	330	0.02	0.19	2.2
Danaus plexippus (Nymphalidae)	35	30	31	210	0.02	0.28	2.5
Zerynthia polyxena (Papilionidae) (Tsai et al., 2014)	32	8.8	27	230	0.02	0.27	3.1
Agathymus polingi (Hesperiidae) (Tsai et al., 2014)	26.7	3.3	7.6	280	0.017	0.1	3.2
Nymphidium sp. (Riodinidae) (Tsai et al., 2014)	26.2	5.2	17.1	120	0.03	0.21	4.8
Cydia pomonella (Tortricidae) (Krenn and Kristensen, 2004)	21	5.3	14	85	0.03	0.2	5.7
Satyrium spini (Lycaenidae) (Tsai et al., 2014)	23	6.3	20	84	0.03	0.28	6.1
Heliothis virescens (Noctuidae)[e]	30	7.9	17	62	0.017	0.18	7.2
Synanthedon vespiformis (Sesiidae) (Krenn and Kristensen, 2004)	27	4.5	28.5	100	0.017	0.34	8.7
Hypena proboscidalis (Erebidae) (Krenn and Kristensen, 2004)	17.8	3.2	14.5	28	0.04	0.26	14
Ethmia dodecea (Depressariidae) (Krenn and Kristensen, 2004)	15.4	3.8	19.3	42	0.017	0.4	20

[a] T_{ref} and Q assume equal permeability for each species, $k = 10^{-15}$ m^2, (Monaenkova et al., 2012). T_{ref} is defined in Eq. (12).
[b] For the reference, we use viscosity and surface tension of water $\eta = 10^{-3}$ Pa s, $\sigma = 0.07$ N m^{-1}.
[c] The permeability of the legular band might be an order of magnitude larger compared with that of the Monarch butterfly (*Danaus plexippus*).
[d] Data are extracted from micrographs published in (Krenn, 2010; Zhang et al., 2018; Krenn and Bauder, 2018; Tsai et al., 2014; Krenn and Kristensen, 2004).
[e] Unpublished data.

$$qw = -\frac{kw}{\eta}\frac{p - p_{atm}}{l} = \frac{kw}{\eta l}\frac{\sigma}{R - h} \tag{3}$$

We call the factor

$$K_{lb} = \frac{kw}{\eta l} \tag{4}$$

the conductivity of the legular band, K_{lb}; it has the physical meaning of the volumetric flow rate per unit length of the proboscis per unit pressure differential. Three morphological parameters of the proboscis determine this conductivity: k, w, and l.

Film conductivity. The film conductivity can be introduced within the framework of the lubrication approximation (Batchelor, 2000) when the radial flow velocity is much smaller than the angular velocity. When the mean film thickness is much smaller than the food canal radius, this approximation is justified. The lubrication approximation assumes that the flow in thin films is almost unidirectional and the angular velocity profile is parabolic through the film thickness (Vogel, 2003, 1996; Batchelor,

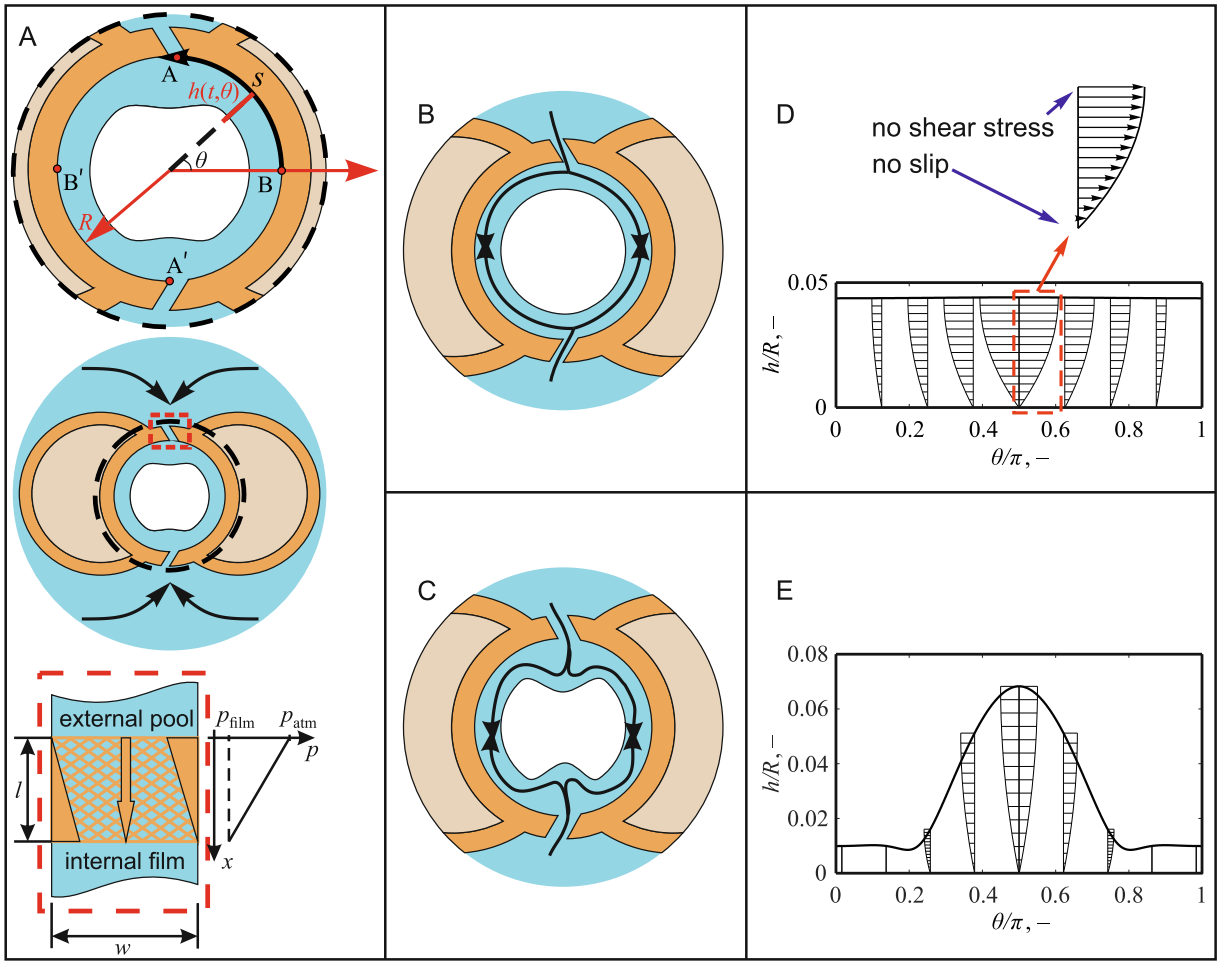

Fig. 3. (A) Schematics of spontaneous fluid flow through the permeable bands of a proboscis into the food canal of circular cross-section. The liquid is shown in blue. The red horizontal arrow is the reference axis ($\theta = 0$) of the polar system of coordinates with the origin at the center of the food canal; the positive angular direction is counterclockwise. The liquid penetrates the proboscis through the dorsal ($\theta = \pi/2$) and ventral ($\theta = -\pi/2$) sides and forms a film covering the surface of the food canal. The boxed magnified schematic shows the linear pressure distribution through the legular band. The pressure in the pool is p_{atm}. The pressure in the film p is lower due to the surface tension of this film. This pressure gradient pushes the liquid from the pool to fill the food canal, as shown by the black arrows. $s = \theta R$ is the arclength along the food canal surface. (B) An enlarged image of the food canal with the adjacent liquid. An illustrative stream line (black) and arrows show the direction of velocity vectors at the points where two streams enter the food canal and where they meet. In this flow scenario, the permeability is very low and hence the velocity component parallel to the wall of the food canal is much greater than the radial component. The air/liquid interface is a circular cylinder co-aligned with the food canal. (C) When the permeability is large, the radial and angular velocity components are comparable in magnitude. In this flow scenario, the air/liquid interface is significantly deformed and no longer circular. (D, E) An unfolded air/liquid interface with the velocity field along the arclength $0 < s < \pi R$, i.e., the arc segment BAB'. The vertical lines show the angular position θ along the food canal where the corresponding parabolic velocity distribution is calculated. The horizontal segments correspond to the absolute value of velocity at each position through the film thickness. The horizontal segments, and hence the flow velocity, disappear as one moves to point B ($\theta = 0$)and its mirror symmetric point B' ($\theta = \pi$).The maximum velocity is observed at point A ($\theta = \pi/2$)and its mirror symmetric point A'($\theta = 3\pi/2$)where the liquid enters the food canal. The parabolic velocity profiles are calculated within the lubrication approximation introduced in Section 5.1. (D) Illustrates the case of a uniform film. (E) Illustrates the velocity distribution at the bump and its vicinity at points A and A' where the liquid enters the film at the legular band. (For interpretation of the references to color in this figure legend, the reader is referred to the web version of this article.)

2000). In Fig. 3D, we schematically show this velocity distribution: the no-slip boundary condition at the wall of the food canal requires the velocity to be zero there, and the maximum velocity is reached at the liquid/air interface where the shear stress is zero. The mean angular velocity v_θ through the film of thickness h is written in the differential form of Darcy's law (2) as

$$v_\theta = -\frac{k_f}{\eta}\frac{\partial p}{\partial(R\theta)}, \quad k_f = h^2/3 \tag{5}$$

where k_f is the permeability of the film (Batchelor, 2000). To find the flow discharge through the film cross-section, one needs to multiply (5) by the film thickness h. Therefore, pulling out R from the differential in Eq. (5), we obtain $hv_\theta = -(k_f h/R\eta)\partial p/\partial\theta$. We call the factor

$$K_f = \frac{k_f h}{\eta R} = \frac{h^3}{3\eta R} \tag{6}$$

the conductivity of the film, K_f; it has the physical meaning of the flow rate through the film cross-section per unit length of the proboscis per unit pressure differential.

The ratio of conductivities of the permeable bands and films allows classification of the flow regimes. Using Eqs. (4) and (6), we calculate the ratio of the two conductivities as

$$K_{lb}/K_f = \left(\frac{kw}{\eta l}\right)\Big/\left(\frac{h^3}{3\eta R}\right) = \frac{3kwR}{h^3 l} = Q\left(\frac{R}{h}\right)^3, \quad Q = \frac{3kw}{R^2 l} \tag{7}$$

where Q is a characteristic dimensionless parameter specifying the insect proboscis. It is independent of the fluid properties and deter-

mines the overall dynamics of the fluid uptake. The values of Q for different species are given in Table 1, provided that the permeability is fixed, $k \sim 10^{-15}$ m^2, at the level of the Monarch butterfly's permeability. Q does not change significantly among species, and its order of magnitude is $Q \sim 10^{-6}$. Only *Ethmia dodecea* (Elachistidae), *Synathedon vespiformis* (Sesiidae), and *Hypena proboscidalis* (Noctuidae) have one order of magnitude larger values, $Q \sim 10^{-5}$. This estimate has to be taken cautiously because we do not know the permeability k. Considering the linear dependence of Q on k in Eq. (7), and assuming that the legular bands have slit-like pores with $k = e^2/12$ where the pore opening e varies in the range 100 nm $< e <$ 1 μm ($e = 100$ nm in Monarch butterflies (Monaenkova et al., 2012) and $e \sim 1\mu m$, as seen in SEM micrographs of the dried *Manduca sexta* proboscis (Zhang et al., 2018); Fig. 2C, assuming that the liquid flows parallel to the legulae through the gap formed by the two legular fences), we estimate the permeability to change in the range 10^{-15} m^2 $< k < 10^{-13}$ m^2. We, therefore, conclude that Q in Lepidoptera is expected to vary as $10^{-7} < Q < 10^{-5}$.

Note that the ratio (7) can be less than, greater than, or equal to 1. Thus, two limiting flow scenarios of liquid uptake can be distinguished. For the first limit, the ratio (7) is less than one, $K_{lb}/K_f \ll 1$, and, for the second limit, this ratio is greater than one, $K_{lb}/K_f \gg 1$. The intermediate flow regime, $K_{lb}/K_f \sim 1$, occurs when both conductivities are comparable and hence both flows (i.e., through the legular bands and film) are equally important. While Q and R are fixed for a species, the ratio K_{lb}/K_f is time dependent; it is inversely proportional to the cube of mean film thickness $h(t)$. Thus, this ratio decreases with time from an initially large value, corresponding to $h(0)$, to its lowest value, Q, as $h \to R$. All three flow regimes follow, one after the other at decreasing ratio K_{lb}/K_f, with the progress of liquid uptake.

An intermediate regime of flow is set when both conductivities are of the same order of magnitude, $K_{lb} \sim K_f$. In this case, setting $K_{lb}/K_f = 1$ and solving (7) for the film thickness to the food-canal radius ratio, we obtain

$$h/R \sim Q^{1/3} \tag{8}$$

As shown above, the parameter Q in Lepidoptera varies ($10^{-7} < Q < 10^{-5}$). Therefore, taking $Q \sim 10^{-6}$ as an average, an intermediate regime of flow is expected to occur when the film thickness is about 1% of the food canal radius, $h \approx 0.01R$.

A strong dependence of the K_{lb}/K_f ratio on the current film thickness h in Eq. (7) suggests that the limiting scenario $K_{lb}/K_f \ll 1$ could be observed soon after the intermediate film thickness (8) is established. This limit assumes that the rate of liquid seepage through the permeable bands is much slower than the rate of liquid flow through the film (i.e., the film is sufficiently thick and is able to transport fluid efficiently). Quantitatively, the limit $K_{lb}/K_f \ll 1$ at $Q \ll 1$ implies that the ratio h/R is not very small compared to Q. Setting $K_{lb}/K_f \ll 1$ in Eq. (7), the following inequality $h/R \gg Q^{1/3}$ is established. One expects that at this limit, the film conductivity is so high that all bumps and indentations on the film surface are smoothed out quickly. Thus, a constant capillary pressure (1) is established over a uniform surface of the air bubble shaped as an infinitely long circular cylinder wrapped up by this film. The film thickness $h(t)$ is time dependent and hence the bubble radius $R - h(t)$ is time dependent as well. The corresponding velocity distribution and representative unfolded film profile are shown in Fig. 3E.

When the film thickness is much smaller than that specified by Eq. (8), we have another flow scenario characterized by the conductivity ratio $K_{lb}/K_f \gg 1$. This flow regime describes the first moments of liquid uptake when the flow rate through the legular bands is much stronger than the rate of film spreading and elevation of the film surface. In this time frame associated with the film spreading, a pressure gradient along the film surface is established. This can be seen from the following arguments.

At the permeable bands, the conservation of mass gives $qw = 2v_\theta h$. Using Darcy's laws (2) and (5), we specify the conservation of mass:

$$-\frac{kw}{\eta l}(p - p_{atm}) = -2\frac{k_f h}{\eta R}\frac{\partial p}{\partial \theta}$$

or, in terms of conductivities K_{lb} and K_f, we have

$$p - p_{atm} = 2\frac{K_f}{K_{lb}}\frac{\partial p}{\partial \theta}$$

Since the pressure gradient $\partial p/\partial\theta$ is finite and the inequality $K_{lb}/K_f \gg 1$ holds true, we infer that at the legular bands the pressure is almost atmospheric

$$p|_{\theta=\pi/2} - p_{atm} = 2\frac{K_f}{K_{lb}}\frac{\partial p}{\partial \theta} \sim 0$$

Far from the legular bands where an equilibrium film configuration has been established, the pressure in the film is specified by Eq. (1). Thus, a pressure gradient builds up, spontaneously pulling the liquid from the legular bands toward the sides of the food canal (Fig. 3C). Since the pressure near the legular band is close to atmospheric pressure, the film and hence the wrapped bubble should substantially deflect from its equilibrium profile of a circular cylinder. This implies that liquid entering the food canal will predominantly accumulate near the legular bands, where the film thickness increases more intensively than at the interior sides of the food canal.

4. Fluid uptake by proboscises limited by the resistance of the permeable bands, $K_{lb}/K_f \ll 1$

To appreciate the importance of the resistance of the legular bands to the spontaneous flow caused by the capillary suction pressure of the film (1), we assume that the liquid entering the food canal instantaneously spreads over the internal film. Thus, the angular velocity of liquid in the film is almost zero at the time scale of liquid seepage through the permeable bands. In this model, the capillary pressure in the film is constant along the film surface and the air bubble remaining at the center of the food canal is shaped as a circular cylinder of radius $r = R - h(t)$ at each time moment t. Since the film thickness changes over time, the pressure in the liquid defined in Eq. (2) depends on time, $p = p(t)$. Assuming that the permeability of the dorsal and ventral legular bands are the same, the liquid discharge through these bands per unit time and unit length of the proboscis is simply $2wq$. The cross-sectional area of the food canal occupied by the liquid film is

$$V(t) = \pi\left(R^2 - r^2\right) \tag{9}$$

Therefore, the liquid discharge per unit length of the proboscis is $dV/dt \equiv 2wq$, and from Darcy's law (2) we have

$$\frac{dV}{dt} \equiv -2\pi r(t)\frac{dr}{dt} = -2K_{lb}(p(t) - p_{atm}) = 2K_{lb}\frac{\sigma}{r}. \tag{10}$$

Assuming that at the first moment of application of the proboscis to the liquid the film thickness is much smaller than the food canal radius, we can set the initial condition for differential Eq. (10) as

$$h|_{t=0} \equiv R - r|_{t=0} = 0 \tag{11}$$

Separating the variables in Eq. (10) as $\pi r^2 dr = -K_{lb}\sigma dt$, integrating this equation using the initial condition (11), and recalling the definition (4) of K_{lb}, one obtains

$$\left(1-\frac{h(t)}{R}\right)^3 = 1-\frac{t}{T_{ref}}, \quad T_{ref}=\frac{\pi\eta R}{\sigma}Q^{-1}, \quad Q=\frac{3kw}{R^2 l}. \tag{12}$$

The reference characteristic time, T_{ref}, is the time required to fill in the circular food canal in the filtration dominated regime, starting with the infinitesimally thin film, $h \to 0$. The reference time depends only on the proboscis structural determinants through parameter Q and surface tension and viscosity of the liquid. The cube of the dimensionless bubble radius, $(r/R)^3$, decreases with time linearly and the bubble collapses at time $t = T_{ref}$. At that time, the food canal is expected to be filled with liquid.

Eq. (12) allows us to make a rough estimate of the flow rate of aqueous solutions through the legular bands and then estimate the characteristic time of the food canal filling when $K_{lb}/K_f \ll 1$. The permeability of the dorsal legular band of the Monarch butterfly was measured in Reference (Monaenkova et al., 2012); $k \sim 10^{-15}$ m^2. Taking water with the surface tension $\sigma = 72$ mN.m^{-1} and viscosity $\eta = 1$ mPa.s as a reference fluid, and the proboscis parameters from Table 1 and substituting them in Eq. (3), we estimate the initial uptake velocity in Monarchs as $q \sim 0.1$ mm.s^{-1} at $h = 0$. Thus, the butterfly needs time $T \sim \pi R^2/2wq = 600$ ms to fill the food canal of radius R. To estimate the time of food-canal filling for species in Table 1, we again use a conservative estimate for the permeability range $10^{-15}\text{m}^2 < k < 10^{-13}$ m^2. Observing that q is directly proportional and T_{ref} is inversely proportional to permeability k, the conservative estimates of these parameters are 0.1 mm.s^{-1} $< q <$ 10mm.s^{-1} and 6 ms $< T_{ref} <$ 600 ms.

These estimates show that the time for food-canal filling at the first sip is <1 s. This mechanism suggests the importance of the food-canal opening, as it provides a fast fluid-delivery vehicle for the insect.

5. General model of fluid intake

5.1. Film dynamics in lubrication approximation

We relax the assumption $K_{lb}/K_f \ll 1$ and consider not only the resistance of legular bands, but also the viscous resistance of the film. Thus, the gradient of the local pressure, $p(t, \theta)$, is the driving force of the fluid spreading over the food canal. This gradient is caused by a) the capillary pressure due to deformation of the film profile with respect to its circular cylindrical shape, and b) the pressure variation at the legular bands when the new liquid enters the food canal. As discussed in Section 3, we employ the lubrication approximation, assuming the flow in the film is almost unidirectional and the angular velocity component is much greater than the radial velocity component $\upsilon_\theta >> \upsilon_r$ (Batchelor, 2000; Oron et al., 1997). Taking an infinitesimally small cylindrical annulus of liquid of the local thickness $h(t, \theta)$ with the base $d\theta$, we write for its volume $dV = \underline{U}d\theta$, where according to Eq. (9), $\underline{U} = (R^2 - (R-h)^2)/2$ is the fluid volume per unit of polar angle and unit length along the proboscis axis. The conservation of the liquid volume is

$$\left(\underline{U}|_{t+dt} - \underline{U}|_t\right)d\theta + \left(h\upsilon_\theta|_{\theta+d\theta} - h\upsilon_\theta|_\theta\right)dt = 0 \tag{13}$$

Taylor expanding the terms taken at $t + dt$ and $\theta + d\theta$ and truncating the Taylor series at the second terms, we have

$$\left(h\upsilon_\theta|_{\theta+d\theta} - h\upsilon_\theta|_\theta\right)dt \approx \frac{\partial(h\upsilon_\theta)}{\partial\theta}d\theta dt \tag{14}$$

$$\left(\underline{U}|_{t+dt} - \underline{U}|_t\right)d\theta \approx \frac{\partial \underline{U}}{\partial t}dtd\theta \tag{15}$$

Substituting (14)–(15) in (13) and dividing the result by $dtd\theta$, Eq. (13) is rewritten as

$$(R-h)\frac{\partial h}{\partial t} + \frac{\partial(h\upsilon_\theta)}{\partial\theta} = 0. \tag{16}$$

Within the assumptions of lubrication approximation, it is natural to consider the porous bands as the infinitesimally thin, widthless slits transporting the liquid at a given flow rate. Substituting Eq. (5) for the mean angular velocity in Eq. (16), we finally obtain the governing equation for film flow along the wall of the food canal

$$(R-h)\frac{\partial h}{\partial t} - \frac{1}{3\eta}\frac{\partial}{\partial\theta}\left(h^3\frac{\partial p}{R\partial\theta}\right) = 0 \tag{17}$$

The Laplace equation of capillarity is taken in the form

$$p - p_{atm} = -\frac{\sigma}{R-h}\left(1 + \frac{\partial}{\partial\theta}\left(\frac{1}{R-h}\frac{\partial h}{\partial\theta}\right)\right) \equiv -\sigma\kappa(t,\theta) \tag{18}$$

This expression, being sufficiently simple to use in numeric analysis, approximates the exact form of capillary pressure

$$p - p_{atm} = -\sigma\left(\frac{1}{(R-h)|\nabla F|} + \frac{1}{R-h}\frac{\partial}{\partial\theta}\left(\frac{1}{(R-h)|\nabla F|}\frac{\partial h}{\partial\theta}\right)\right)$$

$$\nabla F = \left(1; \frac{1}{R-h}\frac{\partial h}{\partial\theta}\right), \quad F(\rho,\theta) = \rho - (R - h(t,\theta)) = 0$$

quite well and allows us to study thin and thick films.

To pose the problem for the second-order partial differential equations (17)–(18), one requires two boundary conditions for each function, h and p, and one initial condition for h. As seen from Table 1, the thickness w of the legular bands is much smaller than the perimeter of the wall of the food canal for each galea, $w/\pi R \sim 0.1$. As shown in Reference (Kiradjiev et al., 2019) for a film spreading over a planar substrate, only the first initial dynamics of spreading are affected by the width of the porous band. We expect that the food-canal curvature does not significantly change this conclusion, and we ignore these first events of fluid penetration through the slits. The effect of the slit width is beyond the lubrication approximation and a detailed flow analysis including the radial component of velocity is required.

Since the C-faces of the galeae are mirror-symmetric, the flow in the films over the right and left galeae should look the same. Moreover, since we assumed the permeabilities of the ventral and dorsal legular bands are the same, the flows from these bands are counter-directed and the liquid streams move toward the sides of the galeae, points $B(\theta = 0)$ and B' $(\theta = \pi)$ (Fig. 3A), where both streams meet. To describe the details of the flow in the vicinity of points B and B', one has to conduct a detailed analysis of flow where the radial component of velocity cannot be ignored. Again, similarly to the permeable slits, these points are the singular points for the lubrication approximation and the associated flow is beyond the scope of our investigation.

The flow between points A and B in Fig. 3A is a representative element of symmetry. This flow is described by Eqs. (17)–(18) in the domain $0 < \theta < \pi/2$. Within the lubrication approximation, we can state that at the point B $(\theta = 0)$ where both streams meet, the film cannot form any cusps and the angular component of velocity is zero; therefore, as follows from Darcy's law, the pressure gradient must be also zero:

$$\left.\frac{\partial h}{\partial\theta}\right|_{\theta=0} = 0, \quad \left.\frac{\partial p}{\partial\theta}\right|_{\theta=0} = 0 \tag{19}$$

At the point A ($\theta = \pi/2$), where the liquid enters the food canal, the film cannot form any cusps and the flow discharge per unit time is related to the pressure drop by Eq. (2). Thus, the boundary conditions at $\theta = \pi/2$ are written as

$$\left.\frac{\partial h}{\partial \theta}\right|_{\theta=\pi/2} = 0, \quad -\left.\left(\frac{h^3}{3\eta}\frac{\partial p}{R\partial\theta}\right)\right|_{\theta=\pi/2} = \frac{qw}{2} \equiv \frac{kw}{2\eta l}\left(p|_{\theta=\pi/2} - p_{atm}\right) \tag{20}$$

The factor ½ in the second condition (20) shows that the flow discharge through the legular band is equally partitioned between the two sides of the food canal.

To formulate the initial condition for this problem, we assume that at the first moment the film of very small thickness h_0 has already been formed at the surface of the food canal and the Laplace capillary pressure (1) has been spontaneously built:

$$h|_{t=0} = h_0, \quad (p - p_{atm})|_{t=0} = -\frac{\sigma}{R - h_0} \tag{21}$$

Thus, the system (17)–(21) constitutes the mathematical model of fluid uptake by a lepidopteran proboscis.

To model proboscises with a single permeable slit situated at $\theta = \pi/2$, one can expand the flow domain to $-\pi/2 < \theta < \pi/2$ and reset the boundary condition (19) at $\theta = -\pi/2$ where the two streams meet.

The model (17)–(21) has been solved using the implicit finite difference method on a uniform grid as detailed in Supplementary Information (SI).

Since Eq. (16) represents the conservation of liquid volume in the infinitesimally thin segment $[R–h;\ R] \times [\theta;\ \theta + d\theta]$, one can deduce the limiting model (10) and (11) or its solution (12) from the general model (17)–(21) by integrating Eq. (17) over the flow domain $0 < \theta < \pi/2$ as

$$4\int_0^{\pi/2}(R-h)\frac{\partial h}{\partial t}d\theta = \frac{dV}{dt} = \frac{4}{3\eta}\int_0^{\pi/2}\frac{\partial}{\partial\theta}\left(h^3\frac{\partial p}{R\partial\theta}\right)d\theta = \frac{4}{3\eta}\left(h^3\frac{\partial p}{R\partial\theta}\right)\Big|_0^{\pi/2} \tag{22}$$

The factor 4 takes into account the symmetry of the flow with two equally permeable legular bands, and hence four quadrants with symmetrically identical flows. Substituting the boundary conditions (19)–(20) in (22), we obtain

$$\frac{dV}{dt} = 2\frac{kw\sigma}{\eta l}\kappa|_{\theta=\pi/2} \tag{23}$$

The factor 2 accounts for the two equivalent legular bands. Once the uniformity of the film thickness is introduced, the derivative $\partial h/\partial\theta = 0$ disappears from Eq. (18), and Eq. (23) reduces to Eq. (10). This reduction is justified for a uniform film of any thickness.

When the initial film thickness h_0 is introduced, the dimensionless initial film thickness $H_0 = h_0/R$ together with the previously introduced dimensionless measure of the legular band permeability, Q, set up an engineering metric for classification of the flow regimes. In the next section, we study the conditions when the film resistance, and hence its non-uniformity, controls the filling dynamics and when the permeability of the legular bands controls the filling dynamics.

6. Dynamics of spontaneous filling of the food canal

6.1. Dynamics of food canal filling

Table 1 shows that the characteristic values of Q span the interval $10^{-7} < Q < 10^{-5}$; therefore, we will investigate the dynamics of fluid uptake by proboscises having this range of Q. Certain features of the filling process are best demonstrated with a higher Q. Thus, we studied the uptake at the following range of parameters: $10^{-3} < H_0 < 10^{-1}$ and $10^{-7} < Q < 10^{-4}$. For comparison, two cases were studied: in the first case, we made both ventral and dorsal legular bands functional (Fig. 4A,B). In the second case, only one legular band is kept functional (Fig. 4C,D). As a result, it takes more time for the bump shoulders to meet each other in the second case. Yet, the overall filling time is of the same order of magnitude, $\sim 2T_{ref}$. The factor 2 is explained by the almost two-fold reduction of fluid discharge at the same driving pressure drop as that for the first case when both legular bands are engaged. These calculations show that all bumps and valleys on the film surface disappear as soon as the maximum film thickness reaches the dimensionless value $H = 0.1$ for the first case and $H = 0.2$ for the second case. From that moment on, the film takes on a circular profile. Thus, the model (17)–(21) reproduces the features of lubrication flows in thin non-uniform films and goes further to reproduce the results based on a simplified model (10)–(12), describing the uptake dynamics at the later stage of flow when the film remains circular.

Fig. 4 illustrates the film profiles for two distinguishable regimes of flow at $Q = 10^{-5}$ and $Q = 10^{-4}$; both flows start with initial film thickness $H_0 = 0.01$.

Liquid accumulation in the vicinity of the legular bands has been observed only at the first moments of fluid uptake and only in a few extreme conditions. In these cases, the initial film thickness is so small that the inequality $K_{lb}/K_f \gg 1$ holds true. As discussed in Section 3, these conditions are specific for the first moments of time when the film is very thin. Soon after the flow begins, the film profile takes on a circular shape, and closely follows Eq. (12). This statement applies for both studied cases when either two or one legular bands are functional. The black dashed curves in Fig. 4E specify the boundary for the case of two active legular bands. The curves are plotted according to Eq. (12)

$$\left(1 - \frac{h(t)}{R}\right)^3 = 1 - \left(\frac{t}{T_{ref}} - \Delta\right), \quad h(\Delta T_{ref}) = 0, \quad h((1+\Delta)T_{ref}) = R \tag{24}$$

The initial time moment, i.e., $h = 0$ at $t/T_{ref} = \Delta$, is adjusted. The Δ-increment takes into account the difference of the filling time caused by the bump formation.

Moreover, for the biologically relevant values of Q and $h/R > H_0 > 0.01$, we have $K_{lb}/K_f \ll 1$, and the overall dynamics of fluid uptake are mostly controlled by the conductivity of the legular bands. In this case, the film remains circular in cross-section almost over the entire process of the food-canal filling, and the overall filling time differs from Eq. (12) by <2% as discussed in Section 7.1.

The flow through the thin salivary film develops in the following steps. Initially, a uniform salivary film of an infinitesimally small thickness is assumed to be present in the food canal. The liquid/air interface is circular and Eq. (21) represents the equilibrium capillary pressure before the application of proboscis to the liquid source, $t < 0$. When the proboscis touches the liquid, the suction pressure (20) is created spontaneously at the legular bands. Therefore, the liquid flows through the legular bands and the liquid/air interface forms a bump. In Fig. 5A, this bump is shown at $t/T_{ref} = 0.0035$ by the black solid curve. The corresponding pressure distribution is shown as the black curve in Fig. 5B. It is evident that the pressure propagates as a wave along the film. The pressure perturbation is initially localized near the legular band and far from this band; it remains equal to the initial value, $R(p - p_{atm})/\sigma = -1/(1 - H_0)$.

The film evolution at the first moments of time is controlled by two mechanisms: the capillary forces tend to smooth out all

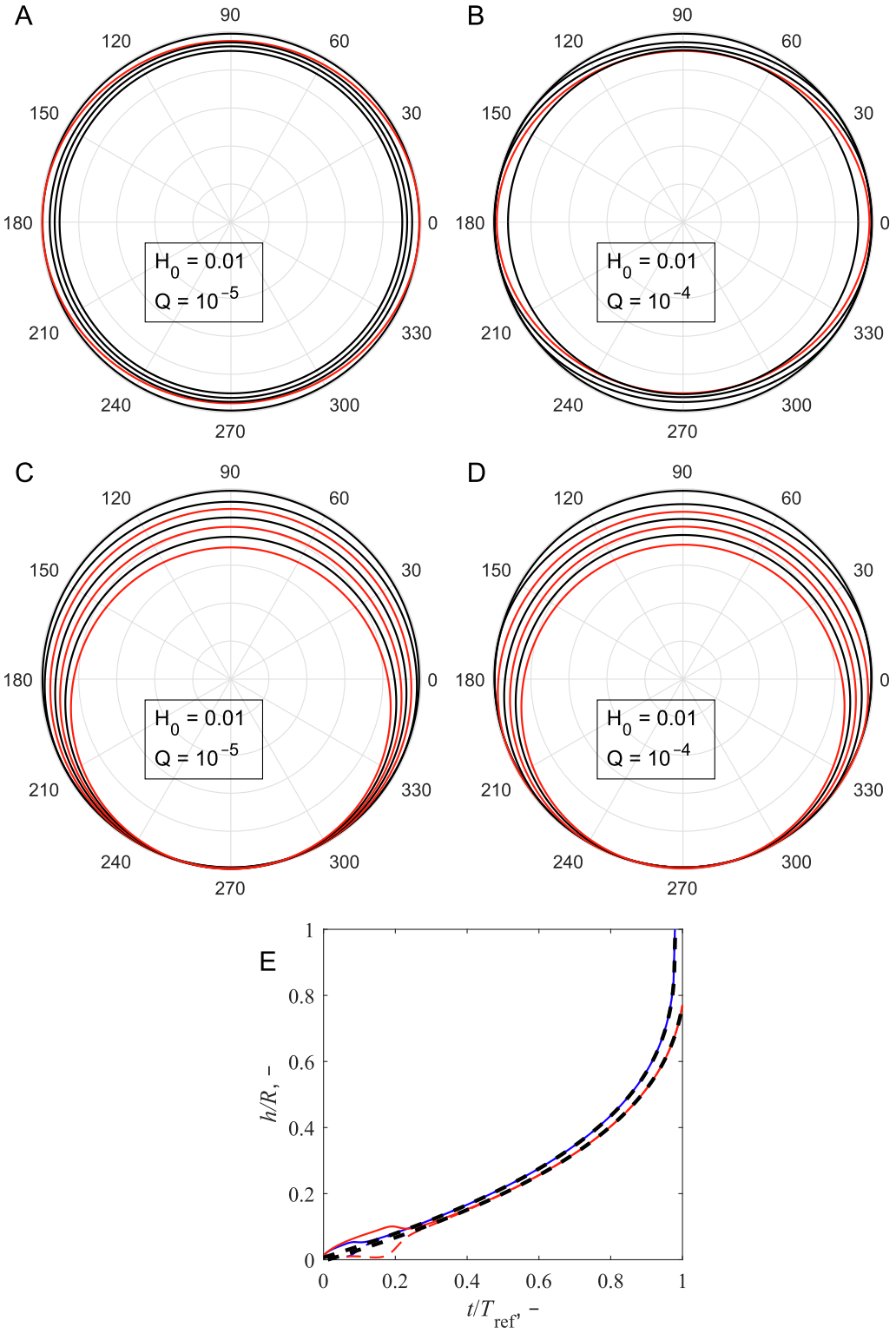

Fig. 4. (A–D) Film profiles in polar coordinates at different time moments, at fixed step calculated using the model (17)–(21) with $H_0 = 0.01$; (A,C) $Q = 10^{-5}$, (B,D) $Q = 10^{-4}$; (A,B) Dorsal and ventral legular bands are functional, time moments $0 < t/T_{ref} < 0.25$, at step 0.0625. At the time moment corresponding to the red curve, the transition between the two limiting flow regimes occurs and the film rapidly takes on a circular shape and becomes almost uniform. From this moment on, the cross-section of the growing film remains circular and hence dependence (12) describes the dynamics of food-canal filling. (C,D) Only one legular band is functional, time moments $0 < t/T_{ref} < 0.75$, at step 0.125. The red profiles are taken at $t/T_{ref} = 0.25$, 0.5, and 0.75. With a single functional legular band, more time is required for the film to spread over the food canal and form a circular profile. The net of the polar system of coordinates is shown at step 0.2 in the radial direction from 0 to 1, and at step 30° in the angular direction from 0° to 360° (see the outer labels).(E) The plot of film thickness at $\theta = \pi/2$ (solid curves) and at $\theta = 0$ (dashed curves) as a function of time for the case of two functional legular bands. The blue ($Q = 10^{-5}$) and red ($Q = 10^{-4}$) curves are calculated using the model (17)–(21) with $H_0 = 0.01$. To match the predictions of the full model, the black dashed curves corresponding to the simplified model (12) were calculated, adjusting the initial conditions according to Eq. (24) where $\Delta = -0.02$ and 0.012 for the upper and lower curves, respectively. (For interpretation of the references to color in this figure legend, the reader is referred to the web version of this article.)

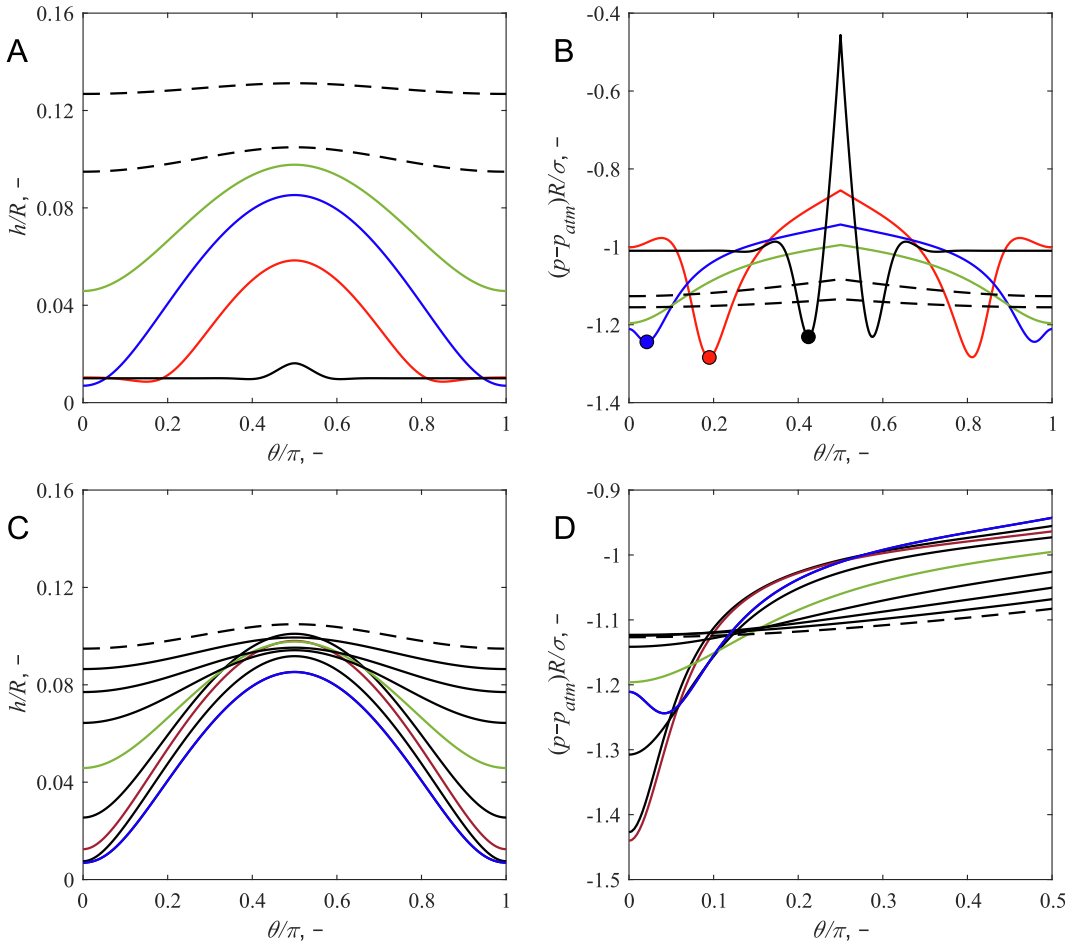

Fig. 5. The characteristic features of the uptake dynamics at $H_0 = 0.01$and $Q = 10^{-4}$. (A) The unfolded film profile h/R and (B) corresponding dimensionless pressure $(p-p_{atm})R/\sigma$ as functions of angular position θ/π at time moments $t/T_{ref} = 0.0035$ (black solid curve), 0.07 (red curve), 0.14 (blue curve), 0.21 (green curve), 0.28, and 0.35 (dashed curves). The marked points in (B) specify the position θ/π in the food canal where the minimum pressure is reached at the given moment of time. (C) The unfolded film profile h/R at different time moments. (D) The corresponding pressure distributions in the films shown in Fig. 5C. These curves illustrate formation of a boundary layer near points B and B' with a high pressure gradient. The greatest pressure gradient is developed at the time moment $t/T_{ref} = 0.1435$ when the minimum pressure is observed at points B and B' (brown curve). The film profiles and pressure distributions are calculated between the time moments 0.14 (blue curves) and 0.28 (dashed curves) at fixed time step 0.0175 for the same conditions as those given in Fig. 5A, B. When the shoulders of two bumps approach each other at points $B(\theta = 0)$ and $B'(\theta = \pi)$ of the food canal, the bump height $h(t, \pi/2)$ demonstrates a non-monotonous behavior. The bump height first increases between the time moments 0 and 0.175 and then decreases for a short period and then continues to increase. The blue, green, and dashed curves correspond to time moment $t/T_{ref} = 0.14$, 0.21, and 0.28, respectively. The black solid curves correspond to the intermediate time moments. (For interpretation of the references to color in this figure legend, the reader is referred to the web version of this article.)

surface perturbations while the entering fluid causes the local bulging of the free surface. Once a small bump forms at the film surface as shown in Fig. 5A by the black solid curve, the pressure in the film at $\theta = \pi/2$ spikes (Fig. 5B). Specifically, the pressure at the bump center instantaneously increases, remaining negative. Simultaneously, the pressure at the bump shoulders dimples down, indicating a stronger suction of the liquid from the bump. As the bump in Fig. 5A grows, expanding its shoulders, the pressure at the bump center decreases, while the peak suction pressures at the bump shoulders move from the legulae towards the leftmost and rightmost points $B(\theta = 0)$and B' $(\theta = \pi)$. Here, the counter-directed mirror symmetric flows from the ventral and dorsal legular bands meet. Two pairs of pressure waves associated with two pairs of symmetric bump shoulders run along the film from points A and A' toward points B and B'. The propagation of a pair of pressure waves from a single legular band is shown in Fig. 5B by the solid curves.

Initially, the two bumps do not interact; that is, their shoulders are far from each other. This can be seen from Fig. 6A and B, where the pressure (Fig. 6A) and the film thickness (Fig. 6B) are shown at point B by the dashed curves for $H_0 = 0.01$ and various Q (see the legend for color interpretation) as functions of time. At an initial time frame $t/T_{ref} < 0.01$ for $Q = 10^{-5}$ and $t/T_{ref} < 0.05$ for $Q = 10^{-4}$ the pressure is almost constant.

The interval of constant pressure is followed by a spike – the rapid increase, decrease, and increase of pressure. The spike amplitude and the time interval of constant pressure both increase with Q and decrease with H_0. The spike indicates the interaction of two bumps, and three phases of the pressure wave development can be distinguished accordingly. At the first phase, when the pressure increases, the two bumps interact through their shoulders while expanding. At the second phase, when the pressure decreases, expansion of bumps slows. As illustrated in Fig. 6B, the second phase ends at $t/T_{ref} = 0.07$ for $Q = 10^{-5}$ and at the time moment $t/T_{ref} = 0.16$ for $Q = 10^{-4}$. The third distinguishable phase of wave propagation starts with the second increase of pressure when the film thickness rapidly increases at point B, and the bump is smoothed out as a result of spontaneous release of liquid from the bump hump towards its shoulders. As a result of this flow, the rate of growth of the bump height slows down during the third

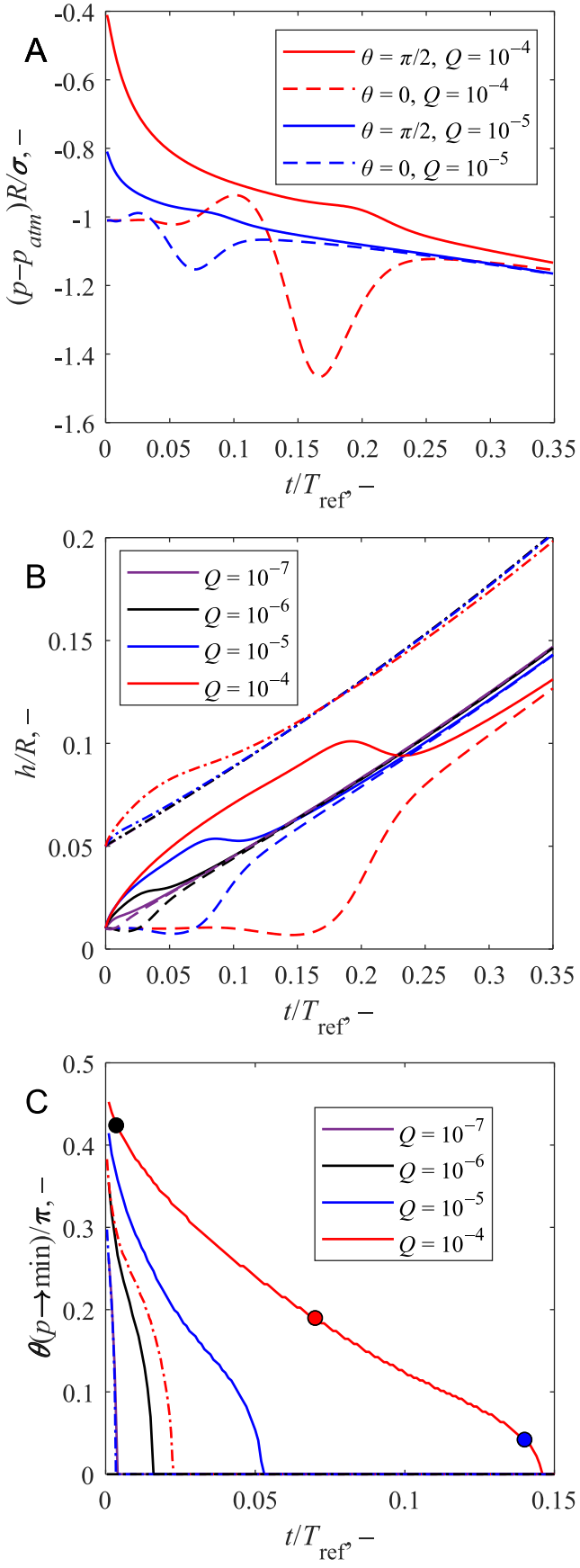

phase, or the height may even decrease. Once the third phase is ended and the pressure relaxed, the film becomes almost circular. The collapse of the circular bubble is described by Eq. (12) fairly well.

7. Discussion

7.1. Characteristic times of food canal filling

Clearly, the overall filling time t_{sc} and the duration of each of the two main stages of fluid flow depend on Q and H_0. Numerical analysis conducted for $10^{-3} < H_0 < 10^{-1}$ and $10^{-7} < Q < 10^{-4}$ using the model (17)–(21) reveals that the overall filling time can be described by the following expression

$$t_{sc}(Q, H_0) = T_{ref}(1 - H_0)^3(1 + \Xi) \tag{25}$$

$$\Xi(Q, H_0) = \frac{3\ln H_0^{-1}}{4\pi(1 - H_0)^3} Q H_0^{-1}$$

The set of (H_0; Q) conditions used for simulations and verification of expression (25) is shown by points in Fig. 7. The corresponding filling times are plotted against expression (25) in Fig. 7B for comparison. In Eq. (25), the factor $(1–H_0)^3$ is introduced to correct Eq. (12) for non-zero initial film thickness. The correction term $\Xi(Q, H_0)$ in parentheses of Eq. (25) is introduced to extend formula (12) and include the effect of fluid flow through a thin film. For very thin films, as $H_0 \to 0$ this term goes to infinity, $\Xi \to \infty$, and the overall filling time becomes independent of Q

$$t_{sc} \sim \frac{\eta R}{\sigma} H_0^{-1} \ln H_0^{-1}, \quad Q \to \infty, \quad H_0 \to 0 \tag{26}$$

This important feature of the model indicates the significance for the food canal of the proboscis to be sufficiently wet. Otherwise, flow resistance through a very thin salivary film would not allow the incoming fluid to spread rapidly over the entire food canal and would jeopardise the efficiency of fluid uptake. The estimate (26) is in agreement with the results of Reference (Kiradjiev et al., 2019) where the authors studied the features of two-dimensional film spreading over a flat surface from a line source. They showed that the time of film spreading scales as $-\ln H_0$.

In Fig. 7A, we show a series of dashed curves – the contour lines $t_{sc}/T_{ref} = const$. The magenta, red, and blue contour lines correspond to $t_{sc}/T_{ref} = 0.97$, 1, and 1.03, respectively. These contour lines span a large (central) region in the (H_0; Q)-plane. In this region between the blue and magenta boundaries, the ratio t_{sc}/T_{ref} is about 1, $t_{sc}/T_{ref} \sim 1$, suggesting that the filling time t_{sc} is almost equal to T_{ref}

Fig. 6. (A) The dimensionless pressure and (B) the dimensionless film thickness as functions of time at points A and B for $H_0 = 0.01$(solid curves correspond to $\theta = \pi/2$ and dashed curves correspond to $\theta = 0$), and for $H_0 = 0.05$(dash-dotted curves correspond to $\theta = \pi/2$; the point $\theta = 0$ is not shown). A slight increase of H_0 from 0.01 to 0.05 makes the bumps and dimples less pronounced. The same effect is caused by a decrease of Q. (C) The position θ/π of the point where the minimum pressure is reached in the film. The markers correspond to the positions of pressure minima in Fig. 5B. The solid curves – $H_0 = 0.01$, the dash-dotted curves – $H_0 = 0.05$. The formation of bumps at $H_0 = 0.05$ and $Q = 10^{-7}$ and at $H_0 = 0.05$ and $Q = 10^{-6}$ is so rapid that it cannot be resolved by the numerical solution at time step $\sim 10^{-4}\ T_{ref}$ and angular step $\sim 0.01\pi$ of integration. Thus, the pressure minimum in the wave moves instantaneously to points B and $B'$and hence the purple and black dash-dotted curves are set at $\theta \equiv 0$. (A–C) $Q = 10^{-4}$ (red curves), $Q = 10^{-5}$ (blue curves), $Q = 10^{-6}$ (black curves), and $Q = 10^{-7}$ (purple curves). (For interpretation of the references to color in this figure legend, the reader is referred to the web version of this article.)

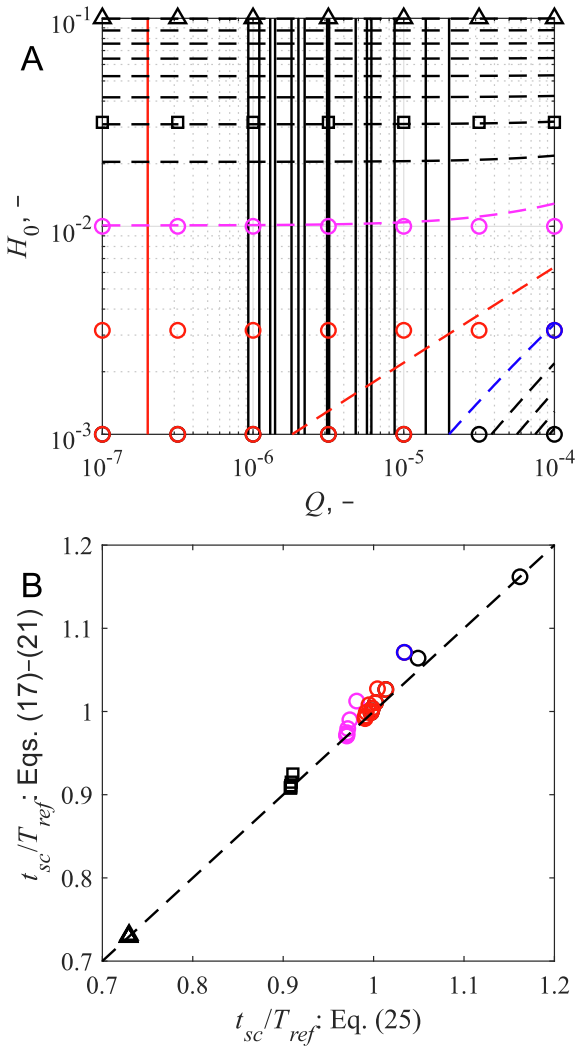

Fig. 7. (A) The subdivision of the (H_0,Q) – plane by the contour lines $t_{sc}/T_{ref} = const$. The dashed contour lines are calculated at the fixed step 0.03, where the uppermost contour line at $H_0 \approx 0.1$ corresponds to $t_{sc}/T_{ref} = 0.73$, while the magenta, red, and blue contour lines correspond to $t_{sc}/T_{ref} = 0.97$, 1, and 1.03, respectively. The lower black inclined contour lines below the blue dashed line are calculated for $t_{sc}/T_{ref} = 1.06$, 1.09, 1.12, and 1.15, respectively. The vertical lines specify the Q values for different lepidopteran species from Table 1 at arbitrary H_0 and fixed $k = 10^{-15} m^2$. The solid red line is also calculated assuming $k = 10^{-15}$ m²for *Manduca sexta* (Sphingidae); it corresponds to the extreme Q value. The species in Table 1 are sorted with respect to the Q-value, in descending order. (B) Numerically calculated overall filling time vs. approximate formula (25). The markers correspond to the same markers on (H_0,Q) – plane in (A). The black triangles and squares and magenta circles group near the ratios $t_{sc}/T_{ref} = 0.73$, 0.91, and 0.97, respectively, in accordance with the corresponding contour lines in (A). All magenta, red, and blue circles lie within the large region between the magenta and blue contour lines in (A) and group closely in (B) suggesting almost the same ratio, $t_{sc}/T_{ref} \approx 1$. (For interpretation of the references to color in this figure legend, the reader is referred to the web version of this article.)

defined by formula (12). Thus, the filling time should not depend on the film thickness H_0 within this domain.

Two more subdomains can be introduced in Fig. 7A: the subdomain situated above the magenta contour line and the subdomain situated below the blue contour line. In the upper subdomain the contour lines are horizontal suggesting that the ratio t_{sc}/T_{ref} is independent of Q. Here, the filling time can be described by the simplified model (25) with $\Xi = 0$. Thus, at the physically reasonable values of Q , the effect of flow along the thin film in the food canal diminishes as $H_0 > 10^{-2}$. In the lower subdomain below the blue contour line, the contour lines are inclined suggesting that both dimensionless parameters H_0 and Q are equally important. However, the results shown in Table 1 suggest that there are no species with H_0, Q values that would fall into this region.

The vertical lines in Fig. 7A specify the Q values for different lepidopteran species from Table 1 at arbitrary H_0 and fixed $k = 10^{-15}$ m², corresponding to the legular bands with slit-like pores having 100-nm openings. With this choice of permeability, fluid uptake is mostly controlled by the permeability of the legular bands.

To evaluate the fluid-uptake scenario for species having larger permeability values, one needs to multiply the given Q by the correction factor for permeability. For example, if the slit-like pores have opening $e \sim 1\mu$m, resulting in permeability $k = 10^{-13}$ m², all the markers on the horizontal Q axis must be multiplied by 100. Therefore, the vertical line for *Manduca sexta* in Fig. 7, $Q = 2 \cdot 10^{-7}$, should be shifted to $Q = 2 \cdot 10^{-5}$. Inspection of species from Table 1 suggests that fluid uptake is mostly controlled by the permeability of the legular bands for any initial film thickness, provided that it is above $0.01R$.

The approximate formula (25) describes all numerical data given in Fig. 7A. The limiting case given by Eq. (26) is beyond the scope of these calculations because it does not reflect the physiological parameters of organisms listed in Table 1.

7.2. Comparison with the conventional mechanism of proboscis filling through an opening at the proboscis tip

The proposed mechanism of fluid uptake by fluid-feeding insects with a lengthwise opening can be compared with the conventional mechanism of fluid filling of a proboscis through an opening at its tip. In the latter case, we can assume that the lumen is open at the proboscis tip and use the Lucas-Washburn theory (Lucas, 1918; Washburn, 1921) to estimate the filling time t_{LW} of a proboscis of length L:

$$t_{LW} = \frac{2\eta L^2}{\sigma R \cos\vartheta_c} \tag{27}$$

where ϑ_c is the contact angle that the fluid makes with the wall of the food canal. Assuming that the food canal is completely wettable by the liquid food, and plugging $\vartheta_c = 0$ in Eq. (27), we can form the ratio t_{LW}/T_{ref} as

$$\frac{t_{LW}}{T_{ref}} = \frac{6}{\pi} Q \frac{L^2}{R^2} \approx 2Q\frac{L^2}{R^2}, \quad Q = \frac{3kw}{R^2 l} \tag{28}$$

which is independent of the liquid properties and depends only on the proboscis characteristics. As estimated earlier, the parameter Q for Lepidoptera changes in the range $10^{-7} < Q < 10^{-5}$. The ratio $(L/R)^2$ for the Monarch butterfly is $(L/R)^2 \sim 10^5$. While the permeability of most lepidopteran species is unknown, the measured permeability for the Monarch suggests that the ratio (28) is about one, $t_{LW}/T_{ref} \sim 1$. The ratio $(L/R)^2$ for *Manduca sexta* is $(L/R)^2 \sim 10^6$ (Zhang et al., 2018; Lehnert et al., 2016) and for the Violet-washed skipper (*Damas clavus*) is $(L/R)^2 \sim 4{\cdot}10^6$ (Lee et al., 2014) Thus, the ratio of filling times for the Lucas-Washburn mechanism of food-canal filling through an opening at the tip and for the proposed mechanism of food-canal filling through lengthwise permeable bands may change within a broad range of $1 < t_{LW}/T_{ref} < 100$. This large ratio indicates that proboscis filling through the lengthwise permeable bands might be advantageous for the insects, or at least, competitive with the mechanism of food-canal filling through a terminal opening. The estimate (27) is optimistic, as it assumes that the proboscis is wide open at the tip and hence there is no resistance to flow through this end. This assumption might be questionable, as the proboscis tip has been

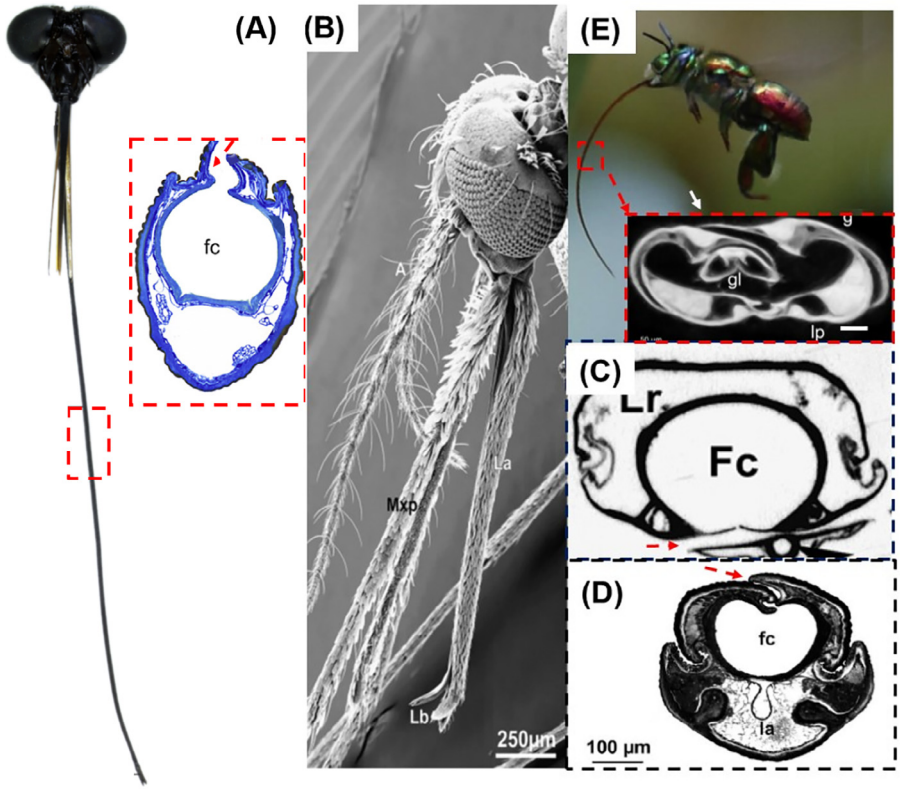

Fig. 8. (A) The distal part of the horse fly proboscis (*Philoliche rostrata*) is responsible for nectar intake. Inset: Cross section of the distal part containing the food canal (fc) closed by a dorsal tongue and groove joint. The red arrow indicates the opening gap for liquid entry into the food canal. Adapted from reference (Karolyi et al., 2014). (B) Head and proboscis of a female mosquito (*Anopheles stephensi*). The piercing structures lie in the scaled sheath. (C). Cross-section of this mosquito and (D) fly proboscises showing the food canal (Fc); the red arrow indicates the opening for liquid entry into the food canal. (B-D) are adapted from references (Krenn and Aspock, 2012; Cerkvenik et al., 2019). (E) Long-tongued orchid bee approaching a flower, with unfolded proboscis. Inset: Micro-CT scan of the proboscis cross-section in resting position; scale bar = 50 μm. The white arrow indicates the opening for fluid entry. Adapted from (Duster et al., 2018). (For interpretation of the references to color in this figure legend, the reader is referred to the web version of this article.)

shown experimentally to be closed but insects can employ different methods to open it partially (Tsai et al., 2014; Monaenkova et al., 2012).

7.3. Biological implications and evolutionary perspectives

A literature survey of many fluid-feeding insects (Krenn, 2019) indicates that their proboscises share similar structural organization: a food canal with slits along its length (Krenn and Aspock, 2012; Krenn, 2019; Krenn and Muhlberger, 2002; Barraclough et al., 2018; Bauder et al., 2013, 2011; Duster et al., 2018; Karolyi et al., 2014, 2012; Cerkvenik et al., 2019). The food canal may have one open lengthwise slit, as in the proboscises of horse flies and mosquitoes (Fig. 8A, B), or it may have two permeable lengthwise bands of slits, as in the proboscises of butterflies and moths (Fig. 8D) and orchid bees (Fig. 8E). This similarity of mouthpart organization in insects from different groups has been largely ignored (Krenn and Aspock, 2012; Krenn, 2010, 2019; Cerkvenik et al., 2019), or at least the functional importance of these openings has not been discussed. We suggest that lengthwise permeable bands connecting the food canal with the fluid increase the efficiency of fluid uptake. Thus, this mechanism of fluid uptake should broaden the opportunistic exploitation of food and water sources, compared with having a drinking straw-type of proboscis with a single terminal opening or a restricted drinking region.

Two critical elements of the proposed feeding mechanism are 1) lengthwise permeability along the proboscis and 2) coating of the food canal walls with a thin film of saliva. In addition to butterflies and moths, long-tongued insects such as bees, certain horse flies, nemestrinid flies, and mosquitoes have gaps along their proboscises (Krenn and Aspock, 2012; Karolyi et al., 2012; Cerkvenik et al., 2019). More generally, the paired nature of haustellate mouthparts, typically assembled after emergence from the pupa (Zhang et al., 2018; Pometto et al., 2020), predispose long-tongued insects to the presence of seams or gaps where the paired structures meet. Permeability along the length of the proboscis has been demonstrated for Lepidoptera (Monaenkova et al., 2012; Kwauk et al., 2014), but permeability data are needed for other groups of long-tongued insects.

A salivary coating of the food canal would be expected in long-proboscis insects, such as butterflies and moths, which use the same channel for salivary discharge and fluid uptake. Similarly, in long-tongued horse flies (*Philoliche*) and nemestrinid flies, the greatly elongated portion of the proboscis (prementum) extends well beyond the separate hypopharynx that contains the salivary duct (Karolyi et al., 2014, 2012). However, in insects with separate channels for saliva delivery and fluid uptake, such as aphids, true bugs, and most blood-feeding insects (Karolyi et al., 2012; Cohen, 1990; Brozek et al., 2015), the potential wetting of the food canal might not apply in a manner similar to that of butterflies and moths. In most blood-feeding insects, and particularly in plant-feeding and predatory insects, the feeding period is considerably longer, often lasting many hours for plant feeders, and the selective value of an enhanced fluid-uptake mechanism, as seen in Lepidoptera, might be minimal. We also note that in some of these plant-feeding and predaceous insects, the coupling mechanism of the mouthparts is elaborate (e.g., Fig. 1 in Cohen (1990)), compared with that of butterflies and moths, and might limit fluid uptake along the length. Perhaps in many insects that pierce plant and animal tissue, selection favors a tighter bundle of mouthparts over

rapidity of fluid uptake. Thus, the proposed mechanism of enhanced fluid uptake along the length of the proboscis might not apply; experimental investigation is needed.

Fluid uptake through lengthwise permeable bands and slits would offer an expanded range of feeding opportunities for insects by providing faster fluid delivery over the entire proboscis length exposed to the fluid. For long-tongued insects, this mechanism might be particularly important, as it would allow them to conserve energy while acquiring fluid (Daniel et al., 1989; Kornev et al., 2017), and for hovering insects, it would decrease the energetic costs of sustained flight while feeding from floral tubes. Lepidoptera with pores or slits along the entire proboscis also would be more efficient in feeding from wet surfaces, such as damp soil or rotten fruit, allowing them to apply much of the proboscis to the liquid surface, rather than acquiring the liquid through a straw-like device with only a terminal opening or with a drinking region in only the distal 5–20%. Thus, the sweeping motion of the proboscis of these surface-film feeders (Knopp and Krenn, 2003) would be coupled with permeability of the legular bands. Long-tongued flies can consume all nectar in a flower when the proboscis is longer than the floral tube (Pauw et al., 2009), suggesting the benefit of porosity along the proboscis.

A more efficient fluid-feeding mechanism should also reduce exposure time to predators if less time were spent conspicuously feeding (e.g., while hovering). If predation has been a strong selection force acting against hovering insects, such as the hawk moth *Xanthopan morganii praedicta*, as they obtain nectar from flowers, the short feeding time (7 s or less) (Wasserthal, 1997; Arditti et al., 2012) would be facilitated if nectar uptake is not limited to the proboscis tip. The nectar column in floral tubes of *A. sesquipedale* is sometimes discontinuous (Wasserthal, 1997) and even if it is only at the bottom of the tube, it would be displaced toward the insect's head as the proboscis enters the column. The nectar, therefore, could be more efficiently and rapidly exploited by a proboscis that is permeable along its length. This advantage positions long-tongued pollinators with lengthwise permeable bands as an evolutionary driving force as plants accommodated unrelated pollinators, each with a longer tongue (Whittall and Hodges, 2007). An additional benefit is accrued by Lepidoptera, which can behaviorally control permeability of the legular bands during feeding by using a variety of proboscis actions, such as anti-parallel movements of the galeae and bending and straightening of the proboscis (Tsai et al., 2014; Kwauk et al., 2014; Zhang et al., 2018, 2019).

For the best-studied examples (i.e., butterflies and moths), we suggest a possible evolutionary scenario illustrating the selective value of enhanced fluid uptake. The earliest fluid-feeding Lepidoptera would not have required linked galeae with porous legular bands. Their short, unlinked, hairy galeae would have allowed them to acquire liquid nourishment and water, via capillarity, from accessible droplets of moisture and gymnosperm fluids (Monaenkova et al., 2012; Kristensen et al., 2007). However, a selective advantage would be gained by those individuals with a proboscis capable of entering crevices to extract liquids. The evolution of angiosperms, particularly floral corollas that held nectar as an energetic reward, would have further selected for more tightly linked galeae (Krenn, 2010; Krenn and Kristensen, 2000). We have argued elsewhere (Pometto et al., 2020) that well-linked galeae are necessary for the proboscis to enter floral tubes as a functional unit. This need is probably especially acute in long-tongued insects that expend energy while hovering. In addition, nectar is not only at the bottom of a flower, but also distributed as films and droplets along the inner walls of the floral tube. An insect with linked galeae, therefore, would benefit from having permeable legular bands along the length of the proboscis, compared with having a single terminal opening or a restricted drinking region. Further fine-tuning of the permeability mechanism could then be achieved with the evolution of behavioral movements of the proboscis to increase or decrease pore size in the legular bands (Tsai et al., 2014; Kwauk et al., 2014).

8. Conclusion

We propose a new mechanism of enhanced fluid uptake by insects, which takes into account an important morphological feature of their proboscises: lengthwise permeable bands. Using Lepidoptera as an example of fluid-feeding insects, we presented the characteristic features of the associated fluid flow and highlighted the importance for the insect to have a food canal wetted with saliva. The salivary film is an important quantitative measure of the enhanced ability of the insect to take up fluid. We showed that fluid uptake will be hindered if the thickness of this saliva film is very small. Quantitatively, this thickness can be estimated by knowing the typical time that the insect spends acquiring liquid (Fig. 7). When the food canal is well wetted with saliva, fluid uptake is mostly controlled by resistance of the permeable lengthwise bands, and the time for filling the food canal is estimated using formula (12).

The proposed mechanism is advantageous especially for long-tongued fluid feeders that use the same canal for saliva discharge and uptake of liquid food and water, as it allows fluid to enter the saliva-wetted food canal along the entire length of the proboscis that is exposed to the fluid. The estimated time of liquid uptake through the apical region of the proboscis would typically be greater for long-tongued Lepidoptera. Moreover, the proposed fluid uptake mechanism reduces the overall amount of energy required to bring fluid to the sucking pump and thence to the digestive system.

CRediT authorship contribution statement

Artur A. Salamatin: Methodology, Software, Formal analysis, Investigation, Writing - original draft, Visualization. **Peter H. Adler:** Visualization, Investigation, Writing - review & editing, Funding acquisition. **Konstantin G. Kornev:** Formal analysis, Visualization, Conceptualization, Methodology, Resources, Writing - original draft, Writing - review & editing, Supervision, Project administration, Funding acquisition.

Declaration of Competing Interest

The authors declare that they have no known competing financial interests or personal relationships that could have appeared to influence the work reported in this paper.

Acknowledgements

A.A.S. acknowledges partial funding from the Russian Government Program of Competitive Growth of Kazan Federal University, and K.G.K acknowledges partial support from SC EPSCoR/IDeA Program under NSF Award no. OIA-1655740. The research by P.H.A. was supported, in part, by the NIFA/USDA under project number SC-1700527; this is Technical Contribution No. 6882 of the Clemson University Experiment Station. The views, perspectives, and content do not necessarily represent those of the SC EPSCoR/IDeA Program, the NSF, or the USDA.

Appendix A. Supplementary data

Supplementary data to this article can be found online at https://doi.org/10.1016/j.jtbi.2020.110525.

References

Adler, P.H., 1982. Soil- and puddle-visiting habits of moths. J. Lepidopterists' Soc. 36, 161–173.

Adler, P.H., Foottit, R.G., 2017. Introduction to Biodiversity. In: Foottit, R.G., Adler, P. H. (Eds.), Insect Biodiversity: Science and Society. . second ed., vol. 1 Wiley-Blackwell, Chichester, pp. 1–7.

Arditti, J., Elliott, J., Kitching, I.J., Wasserthal, L.T., 2012. 'Good Heavens what insect can suck it'- Charles Darwin, *Angraecum sesquipedale* and *Xanthopan morganii praedicta*. Bot. J. Linn. Soc. 169 (3), 403–432.

Barraclough, D.A., Colville, J.F., Karolyi, F., Krenn, H.W., 2018. A striking new species of *Prosoeca* Schiner, 1867 (Diptera: Nemestrinidae): an important pollinator from the Bokkeveld Plateau, Northern Cape Province, South Africa. Zootaxa 4497 (3), 411–421.

Batchelor, G.K., 2000. An introduction to fluid dynamics. Cambridge University Press, New York.

Bauder, J.A.S., Lieskonig, N.R., Krenn, H.W., 2011. The extremely long-tongued Neotropical butterfly *Eurybia lycisca* (Riodinidae): Proboscis morphology and flower handling. Arthropod Struct. Dev. 40 (2), 122–127.

Bauder, J.A.S., Handschuh, S., Metscher, B.D., Krenn, H.W., 2013. Functional morphology of the feeding apparatus and evolution of proboscis length in metalmark butterflies (Lepidoptera: Riodinidae). Biol. J. Linn. Soc. 110 (2), 291–304.

Bennet-Clark, H.C., 1963. Negative pressures produced in the pharyngeal pump of the blood-sucking bug, *Rhodnus prolixus*. J. Exp. Biol. 40 (1), 223–229.

Borrell, B.J., Krenn, H.W., 2006. Nectar feeding in long-proboscid insects. In: Herrel, A., Speck, T., Rowe, N.P. (Eds.), Ecology and Biomechanics: A Mechanical Approach to the Ecology of Animals and Plants. CRC, Boca Raton, pp. 185–205.

Brozek, J., Mroz, E., Wylezek, D., Depa, L., Wegierek, P., 2015. The structure of extremely long mouthparts in the aphid genus *Stomaphis* Walker (Hemiptera: Sternorrhyncha: Aphididae). Zoomorphology 134 (3), 431–445.

Cerkvenik, U., Dodou, D., van Leeuwen, J.L., Gussekloo, S.W.S., 2019. Functional principles of steerable multi-element probes in insects. Biol. Rev. 94 (2), 555–574.

Charnov, E.L., 1976. Optimal foraging, marginal value theorem. Theor. Popul Biol. 9 (2), 129–136.

Cohen, A.C., 1990. Feeding adaptations of some predaceous Hemiptera. Ann. Entomol. Soc. Am. 83 (6), 1215–1223.

Danaher, M.W., Ward Jr., C., Zettler, L.W., Covell Jr, C.V., 2019. Pollinia removal and suspected pollination of the endangered ghost orchid, *Dendrophylax lindenii* (Orchidaceae) by various hawk moths (Lepidoptera: Sphingidae): another mystery dispelled. Florida Entomol. 102 (4).

Daniel, T.L., Kingsolver, J.G., 1983. Feeding strategy and the mechanics of blood sucking insects. J. Theor. Biol. 105 (4), 661–678.

Daniel, T.L., Kingsolver, J.G., Meyhofer, E., 1989. Mechanical determinants of nectar feeding energetics in butterflies-muscle mechanics, feeding geometry, and functional equivalence. Oecologia 79 (1), 66–75.

Davis, N.T., Hildebrand, J.G., 2006. Neuroanatomy of the sucking pump of the moth, *Manduca sexta* (Sphingidae, Lepidoptera). Arthropod Struct. Dev. 35 (1), 15–33.

Duster, J.V., Gruber, M.H., Karolyi, F., Plant, J.D., Krenn, H.W., 2018. Drinking with a very long proboscis: functional morphology of orchid bee mouthparts (Euglossini, Apidae, Hymenoptera). Arthropod Struct. Dev. 47 (1), 25–35.

Eisner, T., 2005. For love of insects. Belknap Press of Harvard University Press, New York, NY.

Grimaldi, D., Engel, M.S., 2005. Evolution of the Insects. Cambridge University Press, New York.

Johnson, S.D., More, M., Amorim, F.W., Haber, W.A., Frankie, G.W., Stanley, D.A., Cocucci, A.A., Raguso, R.A., 2017. Plant-pollinator interactions from flower to landscape. The long and the short of it: a global analysis of hawkmoth pollination niches and interaction networks. Funct. Ecol. 31 (1), 101–115.

Josens, R.B., Farina, W.M., 2001. Nectar feeding by the hovering hawk moth *Macroglossum stellatarum*: intake rate as a function of viscosity and concentration of sucrose solutions. J. Comp. Physiol. A-Sensory Neural Behav. Physiol. 187 (8), 661–665.

Karolyi, F., Szucsich, N.U., Colville, J.F., Krenn, H.W., 2012. Adaptations for nectar-feeding in the mouthparts of long-proboscid flies (Nemestrinidae: *Prosoeca*). Biol. J. Linn. Soc. 107 (2), 414–424.

Karolyi, F., Colville, J.F., Handschuh, S., Metscher, B.D., Krenn, H.W., 2014. One proboscis, two tasks: Adaptations to blood-feeding and nectar-extracting in long-proboscid horse flies (Tabanidae, *Philoliche*). Arthropod Struct. Dev. 43 (5), 403–413.

Kim, W., Gilet, T., Bush, J.W.M., 2011. Optimal concentrations in nectar feeding. PNAS 108 (40), 16618–16621.

Kingsolver, J.G., Daniel, T.L., 1979. Mechanics and energetics of nectar feeding in butterflies. J. Theor. Biol. 76 (2), 167–179.

Kingsolver, J.G., Daniel, T.L., 1995. Mechanics of food handling by fluid-feeding insects. In: Chapman, R.F., de Boer, G. (Eds.), Regulatory mechanisms in insect feeding. Springer, New York, pp. 32–74.

Kiradjiev, K.B., Breward, C.J.W., Griffiths, I.M., 2019. Surface-tension- and injection-driven spreading of a thin viscous film. J. Fluid Mech. 861, 765–795.

Knopp, M.C.N., Krenn, H.W., 2003. Efficiency of fruit juice feeding in *Morpho peleides* (Nymphalidae, Lepidoptera). J. Insect Behav. 16 (1), 67–77.

Kornev, K.G., Adler, P.H., 2019. Physical determinants of fluid-feeding in insects. In: Insect Mouthparts. Springer, Cham, pp. 263–314.

Kornev, K.G., Monaenkova, D., Adler, P.H., Beard, C.E., Lee, W.K., 2016. The butterfly proboscis as a fiber-based, self-cleaning, micro-fluidic system. In: Martin-Palma, R.J., Lakhtakia, A., Knez, M. (Eds.), vol. 9797. Bioinspiration, Biomimetics, and Bioreplication, pp. 263–314.

Kornev, K.G., Salamatin, A.A., Adler, P.H., Beard, C.E., 2017. Structural and physical determinants of the proboscis-sucking pump complex in the evolution of fluid-feeding insects. Sci. Rep. 7, 6582.

Krenn, H.W., 1997. Proboscis assembly in butterflies (Lepidoptera) - a once in a lifetime sequence of events. Eur. J. Entomol. 94 (4), 495–501.

Krenn, H.W., 2010. Feeding mechanisms of adult Lepidoptera: structure, function, and evolution of the mouthparts. Annu. Rev. Entomol. 55, 307–327.

Krenn, H.W., 2019. Insect mouthparts - form, function, development and performance, vol. 5. Springer, Berlin, p. 683.

Krenn, H.W., Aspock, H., 2012. Form, function and evolution of the mouthparts of blood-feeding Arthropoda. Arthropod Struct. Dev. 41 (2), 101–118.

Krenn, H.W., Bauder, J.-A.-S., 2018. Morphological fine tuning of the feeding apparatus to proboscis length in Hesperiidae (Lepidoptera). J. Morphol. 279, 396–408.

Krenn, H.W., Kristensen, N.P., 2000. Early evolution of the proboscis of Lepidoptera: external morphology of the galea in basal glossatan moths, with remarks on the origin of the pilifers. Zool. Anz. 239, 179–196.

Krenn, H.W., Kristensen, N.P., 2004. Evolution of proboscis musculature in Lepidoptera. Eur. J. Entomol. 101, 565–575.

Krenn, H.W., Muhlberger, N., 2002. Groundplan anatomy of the proboscis of butterflies (Papilionoidea, Lepidoptera). Zool. Anz. 241 (4), 369–380.

Krenn, H.W., Zulka, K.P., Gatschnegg, T., 2001. Proboscis morphology and food preferences in nymphalid butterflies (Lepidoptera : Nymphalidae). J. Zool. 254, 17–26.

Kristensen, N.P., Scoble, M.J., Karsholt, O., 2007. Lepidoptera phylogeny and systematics: the state of inventorying moth and butterfly diversity. Zootaxa 1668, 699–747.

Kwauk, K.J., Hasegawa, D.K., Lehnert, M.S., Beard, C.E., Gerard, P.D., Kornev, K.G., Adler, P.H., 2014. Drinking with an unsealed tube: fluid uptake along the butterfly proboscis. Ann. Entomol. Soc. Am. 107, 886–892.

Lauder, G.V., 2003. The intellectual challenge of biomechanics and evolution. In: Bels, V.L., Gasc, J.P., Casinos, A. (Eds.), Vertebrate Biomechanics and Evolution. Springer-Verlag, Berlin, pp. 319–325.

Lechantre, A., Michez, D., Damman, P., 2019. Collection of nectar by bumblebees: how the physics of fluid demonstrates the prominent role of the tongue's morphology. Soft Matter 15 (31), 6392–6399.

Lee, S.C., Kim, B.H., Lee, S.J., 2014. Experimental analysis of the liquid-feeding mechanism of the butterfly *Pieris rapae*. J. Exp. Biol. 217 (11), 2013–2019.

Lee, S.J., Lee, S.C., Kim, B.H., 2014. Liquid-intake flow around the tip of butterfly proboscis. J. Theor. Biol. 348, 113–121.

Lee, S.C., Lee, S.J., 2014. Uptake of liquid from wet surfaces by the brush-tipped proboscis of a butterfly. Sci. Rep. 4, 6934.

Lehane, M.J., 2005. The Biology of Blood-Sucking in Insects. Cambridge University Press, New York.

Lehnert, M.S., Monaenkova, D., Andrukh, T., Beard, C.E., Adler, P.H., Kornev, K.G., 2013. Hydrophobic - hydrophilic dichotomy of the butterfly proboscis. J. R. Soc. Interface 10 (85), 10.

Lehnert, M.S., Beard, C.E., Gerard, P.D., Kornev, K.G., Adler, P.H., 2016. Structure of the lepidopteran proboscis in relation to feeding guild. J. Morphol. 277, 167–182.

Lucas, R., 1918. Ueber das Zeitgesetz des kapillaren Aufstiegs von Flussigkeiten. Kolloid Z. 23, 15–22.

Mollemann, F., Krenn, H.W., Van Alphen, M.E., Brakefield, P.M., Devries, P.J., Zwaan, B.J., 2005. Food intake of fruit-feeding butterflies: evidence for adaptive variation in proboscis morphology. Biol. J. Linn. Soc. 86, 333–343.

Monaenkova, D., Lehnert, M.S., Andrukh, T., Beard, C.E., Rubin, B., Tokarev, A., Lee, W. K., Adler, P.H., Kornev, K.G., 2012. Butterfly proboscis: combining a drinking straw with a nanosponge facilitated diversification of feeding habits. J. R. Soc. Interface 9 (69), 720–726.

Munoz, M.M., 2019. The evolutionary dynamics of mechanically complex systems. Integr. Comp. Biol. 59 (3), 705–715.

Nasto, A., Brun, P.T., Hosoi, A.E., 2018. Viscous entrainment on hairy surfaces. Phys. Rev. Fluids 3 (2), 11.

Oron, A., Davis, S.H., Bankoff, S.G., 1997. Long-scale evolution of thin liquid films. Rev. Mod. Phys. 69 (3), 931–980.

Pauw, A., Stofberg, J., Waterman, R.J., 2009. Flies and flowers in Darwin's race. Evolution 63 (1), 268–279.

Pometto, S., Beard, C.E., Gerard, P., Kornev, K.G., Adler, P.H., 2020. Self-repair of the lepidopteran proboscis. Ann. Entomol. Soc. Am. 113 (1), 6–14.

Russell, E.S., 1916. Form and Function. John Murray, London.

Shaw, S.R., 2014. Planet of the Bugs. The University of Chicago Press, Chicago, p. 240.

Shi, L.H., Wu, J.N., Krenn, H.W., Yang, Y.Q., Yan, S.Z., 2020. Temporal model of fluid-feeding mechanisms in a long proboscid orchid bee compared to the short proboscid honey bee. J. Theor. Biol. 484, 9.

Smith, J.J.B., 1979. Effect of diet viscosity on the operation of the pharyngeal pump in the blood-feeding bug *Rhodnius prolixus*. J. Exp. Biol. 82, 93–104.

Smith, J.J.B., 1985. Feeding mechanisms. In: Kerkut, G.A., Gilbert, L.I. (Eds.), Comprehensive Insect Physiology, Biochemistry and Pharmacology, vol. 4. Pergamon Press, New York, pp. 33–85.

Tsai, C.-C., Mikes, P., Andrukh, T., White, E., Monaenkova, D., Burtovyy, O., Burtovyy, R., Rubin, B., Lukas, D., Luzinov, I., Owens, J.R., Kornev, K.G., 2011. Nanoporous

artificial proboscis for probing minute amount of liquids. Nanoscale 3, 4685–4695.
Tsai, C.-C., Monaenkova, D., Beard, C.E., Adler, P.H., Kornev, K.G., 2014. Paradox of the drinking-straw model of the butterfly proboscis. J. Exp. Biol. 217, 2130–2138.
Vogel, S., 1996. Life in Moving Fluids: The Physical Biology of Flow. Princeton University Press, Princeton, NJ, p. 484.
Vogel, S., 2003. Comparative Biomechanics: Life's Physical World. Princeton University Press Princeton, NJ, p. 582.
Wainwright, P.C., 2007. Functional versus morphological diversity in macroevolution. Annu. Rev. Ecol. Evol. Syst. 38, 381–401.
Washburn, E.W., 1921. The dynamics of capillary flow. Phys. Rev. 17, 273–283.
Wasserthal, L.T., 1997. The pollinators of the Malagasy star orchids *Angraecum sesquipedale*, *A. sororium* and *A. compactum* and the evolution of extremely long spurs by pollinator shift. Botanica Acta 110 (5), 343–359.
Westneat, M.W., Socha, J.J., Lee, W.K., 2008. Advances in biological structure, function, and physiology using synchrotron x-ray imaging. Annu. Rev. Physiol. 70, 119–142.
Whittall, J.B., Hodges, S.A., 2007. Pollinator shifts drive increasingly long nectar spurs in columbine flowers. Nature 447 (7145), 706–U12.
Wigglesworth, V.B., 1972. The life of insects. Weidenfeld and Nicolson:, New York, p. 359.
Zhang, C.Q., Adler, P.H., Monaenkova, D., Andrukh, T., Pometto, S., Beard, C.E., Kornev, K.G., 2018. Self-assembly of the butterfly proboscis: the role of capillary forces. J. R. Soc. Interface 15 (144), 20180229.
Zhang, C.Q., Beard, C.E., Adler, P.H., Kornev, K.G., 2018. Effect of curvature on wetting and dewetting of proboscises of butterflies and moths. *Royal Society Open*. Science 5 171241.
Zhang, C.Q., Adler, P.H., Kornev, K.G., 2019. Insect solutions for open self-cleaning microfluidics. Adv. Mater. Interfaces 6, 1901516.